Large Eddy Simulation of Particulate Turbulent Channel Flows

by

Koji Fukagata
FaxénLaboratoriet

February 2000
Technical Reports from
Kungl. Tekniska Högskolan
FaxénLaboratoriet
S-100 44 Stockholm, Sweden

Typsatt i $\mathcal{AMS}$-LaTeX med KTHs *thesis*-stil.

Akademisk avhandling som med tillstånd av Kungliga Tekniska Högskolan i Stockholm framlägges till offentlig granskning för avläggande av teknologie doktorsexamen fredagen den 11:e februari kl 13.15 i Kollegiesalen, Administrationsbyggnaden, Kungliga Tekniska Högskolan, Valhallavägen 79, Stockholm.

Högskoletryckeriet, Stockholm 2000

Fukagata, K., 2000. Large Eddy Simulation of Particulate Turbulent Channel Flows.
FaxénLaboratoriet, Kungl. Tekniska Högskolan
S-100 44 Stockholm, Sweden

Abstract

This thesis deals with numerical simulations of particulate turbulent channel flows. Turbulent velocity field is simulated using large eddy simulation (LES). Individual particles are tracked by integrating the particle equation of motion, i.e. Lagrangian particle tracking (LPT).

Simulations are first performed with one-way coupling; namely that influence of particles on fluid field is neglected. The methodology is assessed through comparisons between statistics computed for 70 μm copper particles and 50 μm glass particles in a turbulent channel flow of air at $Re_\tau = 180$ and earlier data computed using similar methodology. Good agreement is found between these computational results. Motion of 0.01 μm - 10 μm graphite particles in a channel flow of air at $Re_\tau = 180$ is also simulated. The computed deposition velocity is found to be in good agreement with the empirical relation. In both simulations above, the computed statistics are used to study the importance of different forces acting on the particle.

Subsequently, modulation of turbulence by the presence of 70 μm copper and 50 μm glass particles in a turbulent channel flow of air at $Re_\tau = 180$ is studied by simulations taking into account the force from particles to fluid, i.e. two-way coupling.

Finally, influences of inter-particle collisions are investigated. Simulations of 70 μm particles in a channel flow of air at $Re_\tau = 644$ are compared with the experimental data by Kulick et al.[1] with which all earlier simulation have shown poor agreement. Inter-particle collisions are found to have significant effects on the particle statistics in whole channel even when the particle mass flow ratio is as low as 2%. Agreement with the experimental data can significantly be improved by taking into account inter-particle collisions and a mechanism which prohibits direct re-entrainment of particles from the near-wall region to the bulk flow.

The thesis consists of a survey including required development time for the flows, force balances in the particle phase, modulations in the carrier fluid turbulence due to the presence of particles, particle deposition to walls, passive scalar turbulence, inter-particle collisions, increase of drag coefficient and boundary conditions, followed by seven papers describing specific results.

Descriptors: Turbulence; Two-phase flow; Particle; Channel flow; Large eddy simulation; Lagrangian particle tracking; Deposition; Two-way coupling; Collision.

[1] Kulick, J. D., Fessler, J. R. & Eaton, J. K., 1994. *J. Fluid Mech.* **277,** 109-134.

Preface

This thesis deals with numerical simulations of particulate turbulent channel flows, using large eddy simulation and Lagrangian particle tracking methodology. The thesis is based on the following papers:

Paper 1. GURNIKI, F., FUKAGATA, K., ZAHRAI, S. & BARK, F. H., 2000. LES of turbulent channel flow of a binary electrolyte. To appear in *J. Appl. Electrochem.*.

Paper 2. FUKAGATA, K., ZAHRAI, S. & BARK, F. H., 1997. Large eddy simulation of particle motion in a turbulent channel flow. *Proc. 1997 ASME Fluids Eng. Div. Summer Meeting* (CD-ROM), Paper No. FEDSM97-3591, 1-6.

Paper 3. FUKAGATA, K., ZAHRAI, S. & BARK, F. H., 2000. Dynamics of Brownian particles in a turbulent channel flow. Submitted to *Fluid Dynam. Res.*.

Paper 4. FUKAGATA, K., ZAHRAI, S. & BARK, F. H., 1998. Force balance in a turbulent particulate channel flow. *Int. J. Multiphase Flow* **24**, 867-887.

Paper 5. FUKAGATA, K., ZAHRAI, S. & BARK, F. H., 1998. Fluid stress balance in a turbulent particulate channel flow. *Proc. 3rd Int. Conf. Multiphase Flow* (CD-ROM), Paper No. 157, 1-8.

Paper 6. FUKAGATA, K., ZAHRAI, S., BARK, F. H. & KONDO S., 1999. Influence of the near-wall drag correction in a Lagrangian simulation of particulate turbulent channel flow. *Turbulence and Shear Flow Phenomena - 1* (Eds. Banerjee, S. & Eaton, J. K., ISBN 1-56700-135-1), Begell House Inc., New York, 259-264.

Paper 7. FUKAGATA, K., ZAHRAI, S., KONDO S. & BARK F. H., 2000. Anomalous velocity fluctuations in particulate turbulent channel flow. Submitted to *Int. J. Multiphase Flow.*

Other reports related to this thesis:

Report 1. FUKAGATA, K. 1995. Simulation of particle motion in a turbulent velocity field, part I. Technical Report, SECRC/KB/TR-95/162E, ABB Corporate Research.

Report 2. FUKAGATA, K. & ZAHRAI, S. 1996. Simulation of particle motion in a turbulent velocity field, part II. Technical Report, SECRC/B/TR-96/107E, ABB Corporate Research.

Contents

CHAPTER 1

Introduction

Since perhaps the first scientific observation on turbulence by da Vinci in 15th century, turbulence has been an attractive research area. Numerous experiments were carried out to understand the characteristics of turbulence and to model it mathematically. The effort put on turbulence research has brought two monumental achievements, i.e. the mixing length model (Prandtl, 1927) and the Kolmogorov spectrum (Kolmogorov, 1941; Oboukhov, 1941).

Despite the enormous effort, turbulence has not fully been understood. According to Tennekes & Lumley (1972), turbulence can be characterized by e.g. irregularity, diffusivity, large Reynolds number, three-dimensional vorticity fluctuations and dissipation. Among others it is the irregularity that makes the deterministic approach difficult. Diffusivity is known to cause rapid mixing of the containments such as heat and particles. The diffusivity of the particles in a turbulent flow is of great interest when a filtering, separating or mixing apparatus is designed.

After the invention of computers, many researchers examined to predict the statistics, such as the mean velocity, of turbulent flows by solving the averaged Navier-Stokes equation. Since the Navier-Stokes equation involves a nonlinear advection term, extra unknowns called Reynolds stresses appear in the averaged equation. Therefore relevant closure models are needed to close the equation.

One of the most popular closure models is the $k-\varepsilon$ model (Jones & Launder, 1972), which is based on the Prandtl's mixing-length theory (Prandtl, 1925). The Reynolds stress is approximated to be the product of the turbulent viscosity and the mean strain rate. The turbulent viscosity is assumed to be proportional to k^2/ε, where k is the turbulent kinetic energy and ε is the dissipation rate which are obtained by solving the transport equations for k and ε. Although the $k-\varepsilon$ model has some disadvantages such that it cannot predict a highly anisotropic flow or a flow under rotation, it is widely used for industrial purposes owing to its simplicity and numerical stability.

During the passed few decades, numerical simulations of turbulent flows without high degree of modeling has been made possible due to the rapid development of computational ability. Direct numerical simulation (DNS) uses very fine computational mesh such that the smallest eddies comparable to the Kolmogorov length scale can be captured. In DNS, the Navier-Stokes equation is solved as it is and there is no need for any closure models. Large eddy simulation (LES) uses also fine

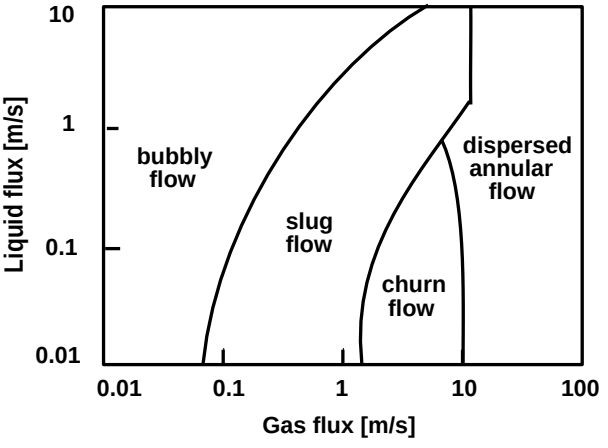

FIGURE 1.1. An example of flow regime map. In the case of gas-liquid flow in a vertical pipe (Mishima & Ishii, 1984).

mesh, but coarser than that in DNS, such that relatively large energetic eddies can be resolved according to a filtered version of Navier-Stokes equation. The relatively large eddies in this context designate the same sizes or larger than those comparable to the integral length scale in the flow. The smaller, subgrid scale (SGS) eddies are considered to be independent of the geometry of the flow and isotropic. Therefore they can be modeled using a SGS model. At the present time, although restricted to relatively lower Reynolds numbers and simple geometries, both DNS and LES are able to reproduce the time dependent turbulent velocity field with a good accuracy.

The nature of turbulence mentioned above will be a hurdle also when the flow consists of two, or more, different phases, i.e. in so called multiphase flows. Turbulent two-phase flows, consisting of e.g. gas and liquid, gas and particle or liquid and particle, can be found almost everywhere from the processes in the nature such as the clouds in the sky, which have existed since long time before mankind appeared on the earth, to the industrial processes such as in the pipes in nuclear reactors which were realized by assembling modern technology.

In general, different phases in two-phase flows interact each other, change the shape of their interface, and transit from one flow pattern to another. For this reason, two-phase flows are usually divided into different flow regimes, which are treated differently. A gas-liquid two-phase flows in a pipe, for instance, can be classified depending on the gas flow rate and the liquid flow rate: bubbly, slug, churn and dispersed annular flow regimes, as shown in Fig. 1.1. The term, dispersed flows, means that one of the phases exists as a dispersed phase. Therefore a bubbly flow is also a kind of dispersed flows.

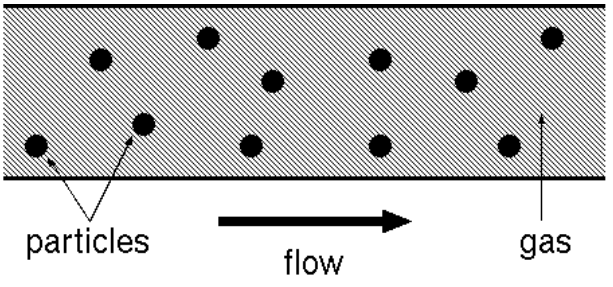

FIGURE 1.2. An example of particulate flow.

In the present thesis, the simplest two-phase turbulent flow which can be studied on a solid basis, i.e. particulate turbulent flow, is chosen for the subject. The particulate flow is a dispersed flow which consist of a fluid as the continuous phase and solid particles as the dispersed phase, as shown in Fig. 1.2. Study of particulate turbulent flows can also be a good starting point for understanding of the mechanisms of more general multiphase turbulent flows.

Difficulty in understanding of particulate turbulent flows arises due to complicated motion of the particles linked to the underlying irregularity of carrier flow turbulence. One exception is the case when the particles have infinitely large inertia compared to the fluid and do not interact with the carrier fluid. In that case particles can be treated similarly to the theory for gas molecules, see Sundaram & Collins (1997). In most cases which are of interest, however, particles do not have infinitely large inertia and do interact with the carrier fluid. Therefore, similarly to the approach for single phase turbulent flow, statistical methods are to be relied on.

There are mainly two different ways to deal with the behavior of particulate turbulent flows: Eulerian-Eulerian approach and Eulerian-Lagrangian approach. The Eulerian-Eulerian approach is often referred to as two-fluid model approach because the particle phase is also treated as a continuum. In the Eulerian-Lagrangian approach, trajectories of individual particles are computed according to the particle equation of motion in the Lagrangian frame, which will be introduced in Chapter 3. The Eulerian-Lagrangian approach is often simply referred to as Lagrangian particle tracking (LPT). It is of course possible to consider Lagrangian-Lagrangian approach. However, Lagrangian approach for the fluid (e.g. Koshizuka et al., 1995, 1998) is only on early stage of development and is not realistic to be used for the computation of turbulent flows.

The simplest particulate turbulent flow is a homogeneous turbulence involving particles. Shih & Lumley (1986) reported on second-order closure modeling of particle dispersion in a decaying homogeneous turbulence. The simulation was found to be in good agreement with the experimental data by Wells & Stock (1983).

Lagrangian particle tracking coupled with DNS (LPT-DNS) of motion of particles in a decaying homogeneous turbulence was performed by Elghobashi & Truesdell (1992) and the important quantities such as Lagrangian velocity auto-correlations and diffusivity of the particles were studied.

Shear flows and jet flows are the next simplest cases because solid boundaries need not to be taken into account. Simonin et al. (1995) developed a second-order closure of the two-fluid model for particulate turbulent shear flows. The time evolution of the various correlations was found to be in good agreement with their data computed using Lagrangian particle tracking coupled with LES (LPT-LES). A turbulent particulate jet flow was simulated by Chen & Wood (1985) using a two-fluid $k-\varepsilon$ model. Effect of the particle size and particle loading on the dispersion was studied by comparing the simulation data with available experimental data by e.g. Boguslawski & Popiel (1979), Wall et al. (1982) and Moderress et al. (1984).

For the practical applications, such as predictions of behaviors of particulate flows appearing in industrial systems, it is necessary to understand the motion of particles in geometries with rigid walls, i.e. wall-bounded flows. The simplest examples with such geometries are straight pipes or channels bounded with two parallel walls. Experimental work on particulate turbulent flows in such pipes or channels has been carried out by many researchers. Laser Dopper anemometry is the most popular technique to observe the motion of particles and was used by e.g. Zisselmar & Molelus (1979), Maeda et al. (1980), Lee & Durst (1981), Tsuji et al. (1984), Kulick et al. (1994) and Kaftori et al. (1995). A high-speed video system was used by e.g. Rashidi et al. (1990) and Niño & Garcia (1996). It was observed in the experiments that the carrier fluid turbulence are suppressed by suspension of small particles and enhanced by large particles. Hetsroni (1989) and Gore & Crowe (1989) summarized the data from the available experiments, and proposed criteria between the enhancement and the suppression of turbulence, which were later validated theoretically by Yuan & Michaelides (1992). It was also found (Fessler et al., 1994) that the particles with finite, small inertia tend to concentrate in the regions with low shear in the streaky turbulent structure near the wall.

Theoretical studies about these wall-bounded particulate flows using numerical simulations have also been reported. The main research interest may be 1) to clarify the phenomena of deposition and entrainment of particles near the wall and 2) to provide statistical moments of particles.

LPT simulation is often used for the prediction of deposition of small particles in a wall-bounded turbulent flow. Ounis et al. (1991) reported on the dispersion and the deposition of very small particles using LPT-DNS. The Brownian motion due to interaction between particles and fluid molecules was also taken into account. The entrainment process was studied by Soltani & Ahmadi (1995) using the same methodology. Deposition in a pipe flow was simulated by Wijttewaal & Oliemans

(1996). Wang & Squires (1996a) used LPT-LES to study particle deposition in a channel. Li & Ahmadi (1993) studied the deposition rate of particles in a channel using a quasi-turbulent fluid velocity field proposed by Kraichnan (1970) as the background turbulence. The same methodology was also applied to the prediction of deposition rate in a complex geometry (Li, et al., 1993). For the cases with very small particles, the simulations mentioned above could predict the statistics such as deposition velocity in good accuracy as compared to the corresponding experimental data (e.g. Liu & Agarwal, 1974) and empirical relation (e.g. Wood, 1981).

LPT simulations for relatively large particles in wall-bounded turbulent flows have also been reported. Pedinotti et al. (1992) carried out a simulation of motion of polystyrene particles with diameters of 120 - 1100 μm in a horizontal water channel using LPT-DNS. The simulation data was compared with the experimental data by Rashidi et al. (1990). Large discrepancies were found. However, later, Pan & Banerjee (1996) revisited the same problem by taking into account the backward influence of particles on fluid, i.e. two-way coupling, and succeeded obtaining statistics in a reasonable agreement with the experimental data by Rashidi et al. (1990).

For the cases where particles have relatively high inertia, such as cases with solid particles of order of 100 μm in wall-bounded air flows, there are still problems remaining on the way for accurate prediction using LPT. Rouson & Eaton (1994) and Wang & Squires (1996b) performed LPT-DNS and LPT-LES, respectively, to simulate the experiments by Kulick et al. (1994) who studied the statistics of 50 μm glass and 70 μm particles in a vertical turbulent channel flow. Although good agreement was found between these computational results, large discrepancies were found as compared to the experimental data. For example, the simulations predicted much lower fluctuation level of particle velocity in wall-normal direction. Similar results were reported by several researchers, e.g. Tanaka et al. (1997).

Simulations using other approaches than LPT have also been reported. Swailes & Reeks (1994) used a kinetic theory for particulate flows (Reeks, 1991) to simulate deposition of particles in a turbulent channel flow and obtained reasonable deposition velocity. Two-fluid models were used by Rizk & Elghobashi (1989), Bolio & Sinclair (1995) and Cao & Ahmadi (1995) to study of turbulent channel flows with relatively heavy and large particles. Bolio et al. (1995) also applied the same model for a complex geometry with risers. Comparison between the model by Rizk & Elghobashi and experiments by Maeda et al. (1980) and Tsuji et al. (1984), for instance, shows that the model by Rizk & Elghobashi has predicted the behavior of particles and fluid reasonably well in the bulk region of the channel, though, discrepancies can be found near the wall. In the other examples simulating heavy and large particles, too, similar agreement and disagreement with experimental data

are reported. For more accurate prediction including the agreement near the wall, further improvement of the existing models is likely to be needed.

To summarize the results of earlier pieces of work, numerical simulations can predict the statistics with a reasonable accuracy when the flow is unbounded, the inertia of particle is small, or both. When the flow is bounded and containing particles with high inertia, the predictability of the simulations is still poor. The poor predictability of both LPT simulation and two-fluid model simulation of wall-bounded turbulent gas-particle flows seems to be due to, at least partly, the same reason. That is a lack of information on what effects must be taken into account and what can be neglected, especially near the walls.

The final goal of this work is to study the motion of particles near the wall, the effect of presence of particles on the turbulent structure near the wall and to make a simple, more accurate model to predict such flows. For these purposes, a computational code to calculate the motion of particles in a turbulent channel flow was developed based on the large eddy simulation code developed by Zahrai et al. (1995). The code was prepared to account for the modulation of the turbulent fluid velocity field due to the presence of particles. Various effects such as particle-particle collisions, increase of drag coefficient near the wall, lift force, Brownian force, etc., are included to examine their importance. Statistics both of the fluid and of the particles are calculated, which will provide the necessary data for the modeling.

This thesis is organized in the following way. In Chapter 2, main ideas behind the large eddy simulation are introduced. Basic concepts and theoretical models on the particle motion follow in Chapter 3. Models for coupling between phases are described in Chapter 4. In Chapter 5, numerical procedures are outlined. Overviews of the papers are presented in Chapter 6. Ideas for the future work are presented in Chapter 7. Finally, in Chapter 8, some general conclusions are drawn. Specific topics are discussed in papers related to this work. The papers are attached to this introductory note. Each paper is in a complete form and can be read also as an independent article.

CHAPTER 2

The model for large eddy simulation

1. Basic concepts

1.1. Basic equations. The governing equation for the motion of an incompressible fluid with a density ρ^f and a kinematic viscosity ν, can be expressed with the continuity equation,

$$\frac{\partial u_i^f}{\partial x_i} = 0 \tag{1}$$

and the Navier-Stokes equation,

$$\frac{\partial u_i^f}{\partial t} = \frac{\partial}{\partial x_j}\left(-u_i^f u_j^f - \frac{1}{\rho}p\delta_{ij} + 2\nu s_{ij}\right) . \tag{2}$$

where u_i^f and p are the velocity and the pressure, respectively. The deformation rate tensor, s_{ij}, is defined as

$$s_{ij} = \frac{1}{2}\left(\frac{\partial u_i^f}{\partial x_j} + \frac{\partial u_j^f}{\partial x_i}\right) . \tag{3}$$

1.2. Direct numerical simulation. A flow becomes turbulent in cases where the nonlinear term in the Navier-Stokes equation, Eq. (2), is sufficiently larger than the viscous term. Turbulence consists of eddies with wide range of length scales. The largest scale is related to a characteristic length in the system, denoted as ℓ. The smallest scale, under which the kinetic energy of the eddies dissipates into thermal energy, is called Kolmogorov length scale, denoted as ℓ_K. Between these two length scales, ℓ and ℓ_K, a scale relation,

$$\frac{\ell_K}{\ell} \sim Re_T^{-3/4} , \tag{4}$$

holds. Here, Re_T is the Reynolds number based on ℓ, ν and the characteristic velocity of the most energetic eddies, u, i.e.

$$Re_T = \frac{u\,\ell}{\nu} . \tag{5}$$

The most primitive and accurate way to compute a turbulent velocity field is to take the size of the computational mesh smaller than ℓ_K and integrate the Navier-Stokes equation directly. This methodology is called direct numerical simulation (DNS). As can be noticed from the scale relation, Eq. (4), the number of mesh

points needed for DNS increases in proportion to $Re_T^{3/4}$ in each direction. If a typical duct flow of air is taken for example and $\ell = 10^{-1}$ m, $u = 1$ m/s and $\nu = 10^{-5}$ m^2/s are assumed, the number of mesh points in one direction can be estimated as $\ell/\ell_K \sim Re_T^{3/4} \simeq 10^3$. In a three dimensional space, one should use 10^9 mesh points by a rough estimate.

1.3. Large eddy simulation. There are interesting characteristics for the eddies smaller than a certain scale, which corresponds to a wavenumber, k_C, on the inertial subrange of the Kolmogorov's energy spectrum. Small scale eddies are rather homogeneous and isotropic regardless of global constraints such as geometrical factors, while the characteristics of the larger eddies are highly dependent on the flow condition. The simulation methodology which utilizes such universal characteristics of small scale eddies is called large eddy simulation (LES). In LES the mesh size is chosen such that it can resolve the larger, geometry- and flow-dependent eddies. The smaller, isotropic eddies are modeled by a subgrid scale (SGS) model. By doing that, the number of computational cells can be reduced. Such decomposition into grid scale field and subgrid scale field was first proposed by Smagorinsky (1963) who studied a quasi-two-dimensional atmospheric turbulence. Since the pioneering work by Deardorff (1970) who applied LES to a channel flow, LES has become an essential tool to study higher Reynolds number turbulent flows than what DNS can handle.

The process to separate the larger, grid scale eddies and smaller, SGS eddies is called filtering. In general, the filtering process of a field, $u_i^f(\vec{x}, t)$, can be expressed with a filtering function, $\mathcal{G}(\vec{x} - \vec{x'})$, i.e.

$$\overline{u_i^f}(\vec{x}, t) = \int u_i^f(\vec{x'}, t)\, \mathcal{G}(\vec{x} - \vec{x'}) d\vec{x'} \ , \tag{6}$$

where $\overline{u_i^f}(\vec{x}, t)$ is the filtered, i.e. grid scale, field.

Among many forms of filtering function proposed in the past, the Gaussian filter, the sharp cut-off filter and the box filter are those mostly used. As is named, the shape of $\mathcal{G}$ of the Gaussian filter is a Gaussian function. The sharp cut-off filter has such a form that the eddies with higher wavenumber than k_C are completely filtered out in the wavenumber space. The box filter works as the volume averaging in the computational cells. Use of different filters leads to need of different SGS models. If the Gaussian filter is used, the SGS model includes so-called Leonard and cross stresses in addition to Reynolds-like stress. Use of the box filter results in a subgrid model close to the classical eddy viscosity concept. The differences in filtered quantities due to choice of filtering operator were studied by Piomelli et al. (1988).

1.4. SGS viscosity. Applying the box filtering, for instance, to the Navier-Stokes equation, Eq. (2), one can obtain an equation for the filtered field, written

as

$$\frac{\partial \overline{u_i^f}}{\partial t} = \frac{\partial}{\partial x_j}\left(-\overline{u_i^f}\,\overline{u_j^f} - \frac{1}{\rho}\overline{p}\delta_{ij} + 2\nu\overline{s_{ij}}\right) + \frac{\partial}{\partial x_j}\left(-\overline{u_i^{f\prime}u_j^{f\prime}}\right) \ , \tag{7}$$

where the over-line expresses the quantity filtered by the box filter and the $u_i^{f\prime}$ denotes the SGS velocity. The last term is the Reynolds-like stress term and can be modeled similarly to the Prandtl's mixing length model (Prandtl, 1925) as

$$R_{ij} = \overline{u_i^{f\prime}u_j^{f\prime}} - \frac{1}{3}\delta_{ij}\overline{u_k^{f\prime}u_k^{f\prime}} = -2\nu_S\overline{s_{ij}} \ . \tag{8}$$

Here, ν_S is the SGS viscosity which has to be modeled using the variables on the filtered scale.

2. SGS model

2.1. Smagorinsky model. The standard SGS model, called Smagorinsky model, can be derived as the following. The transport equation for the SGS kinetic energy, defined by

$$e_S = \frac{1}{2}\overline{u_k^{f\prime}u_k^{f\prime}} \ , \tag{9}$$

can be written as

$$\frac{\partial e_S}{\partial t} + \overline{u_j^f}\frac{\partial e_S}{\partial x_j} = \mathcal{P}_S - \frac{\partial}{\partial x_j}J_{Sj} - \varepsilon_S \ . \tag{10}$$

The first term on the right-hand-side is called production term,

$$\mathcal{P}_S = -\overline{u_i^{f\prime}u_j^{f\prime}}\,\overline{s_{ij}} \ . \tag{11}$$

Since the deformation tensor, s_{ij}, is traceless because of the incompressibility, Eq. (1), the production term can be rewritten using R_{ij} as

$$\mathcal{P}_S = -R_{ij}\,\overline{s_{ij}} \ . \tag{12}$$

The second term in Eq. (10) is the transport term,

$$J_{Sj} = \frac{1}{2}\overline{u_j^{f\prime}u_k^{f\prime}u_k^{f\prime}} + \frac{1}{\rho}\overline{p^\prime u_j^{f\prime}} - 2\nu\overline{s_{ij}^\prime u_i^{f\prime}} \ , \tag{13}$$

and the last term is the viscous dissipation term,

$$\varepsilon_S = 2\nu\overline{s_{ij}^\prime\frac{\partial u_i^{f\prime}}{\partial x_j}} \ . \tag{14}$$

Assuming the production term and dissipation term have much larger magnitude than the transport term such that they balance each other, i.e.

$$\mathcal{P}_S = \varepsilon_S \ , \tag{15}$$

the kinetic energy transport equation, Eq. (10), reduces to

$$-\overline{u_i^{f\prime}u_j^{f\prime}}\,\overline{s_{ij}} = \varepsilon_S \ . \tag{16}$$

Using Eq. (8) and Eq. (16), one obtains an expression for the SGS viscosity as a function of the dissipation rate and the filtered deformation rate, which reads

$$\nu_S = \frac{\varepsilon_S}{2|\overline{s_{ij}}|^2} \ . \tag{17}$$

From a dimensional analysis, ε_S can be estimated using $|\overline{s_{ij}}|$ and the length scale of SGS eddies, ℓ_S, as

$$\varepsilon_S \sim |\overline{s_{ij}}|^3 \ell_S^2 \ , \tag{18}$$

thus

$$\nu_S \sim \ell_s^2 |\overline{s_{ij}}| \ . \tag{19}$$

In the original Smagorinsky model, ℓ_S is taken as the size of the cubic box, Δ. When the computational cell is not a cube but a parallelopipedon, Δ is usually (Miyake, 1992) taken as

$$\Delta = (\Delta x_1 \Delta x_2 \Delta x_3)^{1/3} \ , \tag{20}$$

where Δx_i is the size in i-direction of the cell. In that case, ν_S can be modeled as

$$\nu_S = \sqrt{2}(C_S \Delta)^2 |\overline{s_{ij}}| \ . \tag{21}$$

The constant, C_S, is called Smagorinsky constant.

Lilly (1967) found that C_S is equal to 0.085 under the condition where the computational mesh is sufficiently fine and all the subgrid scale eddies are in the universal range. In numerical simulations, C_S is usually taken between 0.1 and 0.25 depending on the characteristics of the flow (Miyake, 1992).

In a channel flow, C_S is usually taken around 0.12, though, it is known that the Smagorinsky model overestimates the subgrid scale velocity in the vicinity of wall. This shortcoming is usually fixed by use of a damping function such as

$$\nu_S(y^+) = \nu_S \left(1 - \exp(-\frac{y^+}{25}) \right) \ . \tag{22}$$

2.2. Dynamic SGS model. As an approach to avoid artificial adjustments of SGS viscosity, such as use of a damping function, Germano et al. (1991) proposed a dynamic SGS model. The main feature of the dynamic SGS model is use of two different filters, i.e. a grid filter and a test filter with a larger size. The value of C_S can then be dynamically computed using the relation between these different filters.

The dynamic SGS model based on the Smagorinsky model can be derived as the following. The size of the test filter is chosen as $n\Delta$ and the quantity filtered by this is expressed as e.g. $\widehat{u_i^f}$. The subgrid stress, expressed as

$$T_{ij} = \overline{u_i^f}\ \overline{u_j^f} - \overline{u_i^f u_j^f} \ , \tag{23}$$

can be filtered by the test filter to read

$$\widehat{T_{ij}} = \widehat{\overline{u_i^f}\,\overline{u_j^f}} - \widehat{u_i^f u_j^f} \ . \tag{24}$$

On the other hand, the combination of the grid filter and the test filter leads to another subgrid stress, written as

$$\mathcal{T}_{ij} = \widehat{\overline{u_i^f}}\,\widehat{\overline{u_j^f}} - \widehat{\overline{u_i^f u_j^f}} \ . \tag{25}$$

The auxilary quantity,

$$\mathcal{L}_{ij} = \widehat{\overline{u_i^f}}\,\widehat{\overline{u_j^f}} - \widehat{\overline{u_i^f u_j^f}} \ , \tag{26}$$

can then be expressed as

$$\mathcal{L}_{ij} = \mathcal{T}_{ij} - \widehat{T_{ij}} \ . \tag{27}$$

This relation is called as Germano identity. Finally, by performing similar transformations to those done for the derivation of Smagorinsky model, one finds a relation between the Smagorinsky constant, C_S, and the quantity, $\mathcal{L}_{ij}$, as

$$\mathcal{L}_{ij} - \frac{1}{3}\mathcal{L}_{kk} = 2C_S^2 M_{ij} \ . \tag{28}$$

Here M_{ij} is defined as

$$M_{ij} = (n\Delta)^2 |\widehat{\overline{s_{ij}}}|\,\widehat{\overline{s_{ij}}} - \Delta^2 \widehat{|\overline{s_{ij}}|\,\overline{s_{ij}}} \ . \tag{29}$$

As can be seen, this set of equations have too many independent variables for the determination of one variable, C_S. Such mathematical ill-posedness is usually fixed by multiplying $\overline{s_{ij}}$ (Germano et al, 1991), or M_{ij} (Lilly, 1992) on both hand sides of Eq. (29).

In the present study, however, the dynamic SGS model is not adopted just because the turbulent velocity field can be computed with a good accuracy using the modified Smagorinsky model, introduced in the following, without use of any damping function near the wall.

2.3. SGS model in the present study. In the present study, a highly anisotropic computational mesh system is used for the efficiency and accuracy of the computation of a turbulent channel flow. Therefore, a modified version of the Smagorinsky model appropriate for such a mesh system (Zahrai et al., 1995) is used.

Following Deardorff (1970), the local diffusivity in j direction, ν_{Sj}, is assumed to depend on the filtered dissipation, ε_S and the cut-off length scale in j direction, ℓ_{Sj}, i.e.

$$\nu_{Sj} = \varepsilon_S^{1/3} \ell_{Sj}^{4/3} \ . \tag{30}$$

The dissipation rate, ε_S, is estimated using the geometric mean of the side-lengths of the cell, Δx_1, Δx_2, Δx_3, as

$$\varepsilon_S \sim |\overline{s_{ij}}|^3 (\Delta x_1 \Delta x_2 \Delta x_3)^{2/3} \ . \tag{31}$$

The length scale in j-direction, ℓ_{Sj}, is naturally estimated by the smallest resolved scale in j-direction, Δx_j. Substituting these estimations into Eq. (30), ν_{Sj} can be modeled as

$$\nu_{Sj} = \sqrt{2} C_S^2 (\Delta x_1 \Delta x_2 \Delta x_3)^{2/9} (\Delta x_j)^{4/3} |\overline{s_{ij}}| \ . \tag{32}$$

The model constant proposed by Zahrai et al. (1995) is $C = 0.08$.

CHAPTER 3

The model for Lagrangian particle tracking

1. Basic concepts

The basic concept of the Lagrangian particle tracking is to integrate the particle equation of motion, described in the Lagrangian frame, for individual particles. The equation of motion for a particle, labeled by (k), with a mass, m, can be expressed as

$$\begin{cases} \dfrac{dx_i^{p(k)}}{dt} &= u_i^{p(k)} \ , \\ m\dfrac{du_i^{p(k)}}{dt} &= f_i^{(k)} \ , \end{cases} \tag{33}$$

where $x_i^{p(k)}$ and $u_i^{p(k)}$ are, respectively, the component of the location and the velocity of the particle, in the i-direction. For convenience in notation, the particle index, (k), will be dropped, otherwise explicitly specified. The force acting on a particle, f_i, is contributed from three parts:

1. surface forces from surrounding fluid, such as drag, $f_i^{(drag)}$, and lift, $f_i^{(lift)}$;
2. body forces, $f_i^{(body)}$, such as gravitational force;
3. impulsive forces from wall, $f_i^{(wall)}$, and from other particles, $f_i^{(coll)}$;

and can symbolically be expressed as

$$f_i = f_i^{(drag)} + f_i^{(lift)} + f_i^{(body)} + f_i^{(wall)} + f_i^{(coll)} + (other \ \ terms) \ . \tag{34}$$

In the following sections, a general particle equation of motion valid for the cases at low particle Reynolds number is first introduced. After that, various effects specific to the particle with high inertia and the particle in wall-bounded flows are considered.

2. Particle equation of motion

2.1. Stokes drag. It was C. G. Stokes in 19th century who expressed the stream function of the flow around a spherical particle in the cases where the nonlinear term in Navier-Stokes equation is negligibly small compared to the viscous

term. Such case occurs when the particle Reynolds number,

$$Re_p = \frac{|\vec{u}^f - \vec{u}^p|d}{\nu}, \tag{35}$$

where d is the particle diameter, is much less than unity. The drag force, $f_i^{(drag)}$, acting on a non-accelerating particle in a steady and uniform flow can then be obtained using the Stokes stream function as

$$\frac{f_i^{(drag)}}{m} = \frac{1}{\tau_p}(u_i^f - u_i^p) \ . \tag{36}$$

The coefficient, τ_p, is called Stokes relaxation time, defined as

$$\tau_p = \frac{d^2 S}{18\nu} \ , \tag{37}$$

where S is the density ratio of particle to fluid, i.e.

$$S = \frac{\rho^p}{\rho^f} \ . \tag{38}$$

2.2. BBO equation. Basset (1888), Boussinesq (1903) and Oseen (1927) examined the motion of a sphere settling down in a fluid due to gravitational force. The particle equation of motion developed by them is called Basset-Boussinesq-Oseen (BBO) equation. Tchen (1947) extended the BBO equation such that it could describe the particle motion in an unsteady flow. Extension was also examined for non-uniform flows, though, it had some inconsistency as pointed out by Corrsin & Lumley (1956). Later, Buevich (1966) and Riley (1971) made a correction to Tchen's expression.

Maxey & Riley (1983) presented a particle equation of motion for unsteady nonuniform flow, which reads

$$\begin{aligned}
\frac{du_i^p}{dt} &= \frac{1}{\tau_p}\left\{u_i^f - u_i^p + \frac{1}{24}d^2\nabla^2 u_i^f\right\} \\
&+\frac{1}{S}\frac{Du_i^f}{Dt} \\
&+\frac{1}{2S}\frac{d}{dt}\left\{u_i^f - u_i^p + \frac{1}{40}d^2\nabla^2 u_i^f\right\} \\
&+\frac{9\nu}{dS}\int_0^t dt' \left[\frac{\frac{d}{dt'}\left\{u_i^f(t') - u_i^p(t') + \frac{1}{24}d^2\nabla^2 u_i^f(t')\right\}}{\{\pi\nu(t-t')\}^{1/2}}\right] \\
&+\left(1 - \frac{1}{S}\right) g_i \ ,
\end{aligned} \tag{39}$$

where u_i^p represents the instantaneous particle velocity, and u_i^f is the instantaneous fluid velocity at the center of the particle if the particle were not present. The operator, D/Dt, represents a derivative along the fluid path, while d/dt is that along the particle trajectory.

The five terms on the right hand side of the equation are usually referred to as:

1. drag force;
2. fluid acceleration;
3. added mass;
4. history effect;
5. gravitational force.

This expression is relevant for the Stokes flow regime. Note that in the drag force, the added mass and the history effect terms of Eq. (39), a correction term due to the velocity curvature of the carrier fluid called Faxén correction (Faxén, 1924) is included.

A turbulent flow in a channel whose half width is δ is simulated in the present study. Assuming that the characteristic acceleration of fluid can be evaluated by δ and the shear velocity, u_τ, as

$$\left|\frac{D\vec{u}^f}{Dt}\right| \sim \left|\frac{d\vec{u}^p}{dt}\right| \sim \left|\frac{d\vec{u}^f}{dt}\right| \sim \frac{u_\tau^2}{\delta} , \tag{40}$$

the magnitude of the fluid acceleration term in Eq. (39) relative to the dominant drag force can be estimated as

$$\frac{\left|\frac{1}{S}\frac{D\vec{u}_i^f}{Dt}\right|}{\left|\frac{18\nu}{d^2 S}(\vec{u}_i^f - \vec{u}_i^p)\right|} \sim \frac{d^2 u_\tau}{\nu\ \delta} = \left(\frac{d}{\delta}\right)^2 Re_\tau , \tag{41}$$

where Re_τ is the wall-shear Reynolds number, defined by

$$Re_\tau = \frac{u_\tau \delta}{\nu} . \tag{42}$$

The magnitude of other terms in Eq. (39) and the Faxén correction relative to the dominant drag force term can similarly be estimated as shown in Table 3.1. When the diameter of the particle is much smaller than the channel width, as is in the present study, the particle equation of motion can reduce to that consisting only of the drag force and the gravitational force. Furthermore, when the particle is much heavier than fluid as is such in gas-particle flow, the gravitational term can also be simplified to g_i only. Thus, the particle equation of motion for a low particle Reynolds number gas-particle flow in an unbounded flow can be well approximated by

$$\frac{du_i^p}{dt} = \frac{1}{\tau_p}(u_i^f - u_i^p) + g_i . \tag{43}$$

3. Interaction between fluid molecules and small particles

3.1. Slip correction to drag force. When the particle diameter, d, is as small as the mean free path of fluid molecules, λ, the expression of Stokes drag, Eq. (36) with Eq. (37), is no more appropriate due to the slip at the interface between particle and fluid. In such case, the Stokes drag is corrected by the Stokes-Cunningham correction factor, C_C, given as (Davies, 1945)

$$C_C = 1 + \frac{2\lambda}{d}(1.257 + 0.4e^{-1.1d/2\lambda}) \ . \tag{44}$$

The drag is then expressed by Eq. (36) with a corrected relaxation time,

$$\tau_p = \frac{d^2 \ S \ C_C}{18 \ \nu} \ . \tag{45}$$

3.2. Brownian force. When small particles are dealt with, an additional term accounting for the Brownian forces should be added to the particle equation of motion. Assuming that the Brownian force in i-th direction is expressed as a random function, $f_i^{(Brown)}(t)$, the particle equation of motion can be written as a form of Langevin equation, i.e.

$$\frac{du_i^p}{dt} = \frac{1}{\tau_p}(u_i^f - u_i^p) + \frac{f_i^{(Brown)}(t)}{m} \ . \tag{46}$$

Assuming also the time scale for the Brownian motion, τ_B, i.e. time scale related to u_i^p, is much shorter than that for fluid motion, τ_f, related to u_i^f, it can be possible to take a separation time scale, Δt, which satisfies

$$\tau_B << \Delta t << \tau_f \ . \tag{47}$$

In such case, the time derivative of u_i^f has a negligibly small magnitude as compared to that of u_i^p. Therefore the Langevin equation above can be approximated using the relative velocity, $u_i^R = u_i^p - u_i^f$, as

$$\frac{du_i^R}{dt} = -\frac{1}{\tau_p}u_i^R + \frac{f_i^{(Brown)}(t)}{m} \ . \tag{48}$$

TABLE 3.1. Magnitude of each term in the particle equation of motion relative to the drag force term.

Term	Relative magnitude
Fluid acceleration	$\sim (d/\delta)^2 Re_\tau$
Added mass	$\sim (d/\delta)^2 Re_\tau$
History effect	$\sim (d/\delta) Re_\tau^{1/2}$
Faxén correction	$\sim (d/\delta)^2$

Integration of this equation over a time, Δt, gives a general solution,

$$u_i^R(t+\Delta t) = u_i^R(t)\exp\left(-\frac{\Delta t}{\tau_p}\right) + u_i^{(Brown)}(\Delta t) \ , \tag{49}$$

where

$$u_i^{(Brown)}(\Delta t) = \int_t^{t+\Delta t} \frac{f_i^{(Brown)}(t')}{m} dt' \ . \tag{50}$$

The distribution of summation of $u_i^{(Brown)}(t)$ from $t = 0$ to $t = \infty$ should tend to Maxwellian distribution. Therefore $u_i^{(Brown)}(\Delta t)$ should have a distribution, $P[u_i^{(Brown)}(\Delta t)]$, such as (Chandrasekhar, 1943)

$$\begin{aligned} P[u_i^{(Brown)}(\Delta t)] &= \frac{1}{(4\pi kT\Delta t/m\tau_p)^{1/2}} \exp\left(-\frac{|B_i(\Delta t)|^2 m\tau_p}{4kT\Delta t}\right) \\ &\sim N\left(0, \sqrt{\frac{2kT\Delta t}{m\tau_p}}\right) \ , \end{aligned} \tag{51}$$

where $N(0,\sigma_B)$ is the normal distribution with a mean value of 0 and a standard deviation of σ_B. The Brownian force can then be modeled as

$$\frac{f_i^{(Brown)}}{m} = G_i \frac{\sigma_B}{\Delta t} \ , \tag{52}$$

where G_i is a Gaussian random number with zero-mean unit-variance. Note that the final expression, Eq. (52), is the same as that derived by Ounis et al. (1991), who discussed on the spectral intensity of the Brownian force.

4. Higher particle Reynolds number

4.1. Drag force. The Stokes drag, Eq. (36), as well as the drag term that in the particle equation of motion above, Eq. (43), is relevant only for the Stokes regime, i.e. cases where the particle Reynolds number is less than unity. In general, the drag force can be expressed as

$$\frac{f_i^{(drag)}}{m} = \beta(u_i^f - u_i^p) \ , \tag{53}$$

where β is the function of the particle Reynolds number.

For the particle Reynolds number slightly higher than the Stokes limit, an expression called Oseen drag (Oseen, 1927), which is derived by linearizing the Navier-Stokes equation,

$$\beta = \frac{1}{\tau_p}(1 + \frac{3}{16}Re_p) \ , \tag{54}$$

may be useful. The Oseen drag gives reasonable accuracy up to $Re_p \simeq 5$.

For the cases of higher particle Reynolds number, the nonlinearity of the advection term makes analytical derivation of the drag coefficient difficult. For such cases, an empirical drag coefficient proposed by Schiller & Naumann (1933),

$$\beta = \frac{1}{\tau_p}(1 + 0.15Re_p^{0.687}) \ , \tag{55}$$

is widely used. The curve of drag coefficient calculated using this formula have only a few percents of deviation from the standard drag curve.

4.2. Lift force. While the drag force works in the same direction as the flow, the lift force is a lateral force which a particle receives from the surrounding fluid. There are two different mechanisms to produce lift force on a particle:

1. slip-spin lift;
2. slip-shear lift.

The spin-slip lift is due to rotation of the particle and sometime called Magnus lift or Rubinow-Keller force (Rubinow & Keller, 1961). The slip-shear lift is caused by shear of the surrounding fluid, which makes the pressure distribution around the particle non-uniform. As noted by Bretherton (1962), the slip-shear lift force is not produced when the flow is in the Stokes flow regime.

Saffman (1965, 1968) derived the magnitude of slip-shear lift force using inner- and outer expansions of the Navier-Stokes equation. The expression by Saffman, called Saffman lift, can be written as

$$f_2^{(lift)} = 6.46\rho^f \nu^{1/2} \left(\frac{d}{2}\right)^2 (u_1^f - u_1^p) \left|\frac{du_1^f}{dx_2}\right|^{1/2} \operatorname{sgn}\left(\frac{du_1^f}{dx_2}\right) . \tag{56}$$

It was also shown by Saffman that the slip-shear lift for a freely rotating spherical particle is one order of magnitude larger than the spin-slip lift unless the particle rotates extremely fast.

Li & Ahmadi (1994) extended the Saffman lift for a particle in a three-dimensional shear flow by replacing the shear, du_1^f/dx_2, by the deformation tensor, s_{ij}. The lift force in a three-dimensional shear is then expressed as

$$\frac{f_i^{(lift)}}{m} = \frac{5.19\nu^{1/2}s_{ij}}{Sd(s_{lk}s_{kl})^{1/4}}(u_j^f - u_j^p) \ . \tag{57}$$

5. Effects of walls

5.1. Increase of drag coefficient. Drag coefficient is known to be modified near solid walls. As Faxén (1923) derived analytically, using the method of reflections, the drag coefficient in the directions parallel to the wall, denoted here as x and z directions, increases when a particle is located near a plane wall. When the distance between a plane wall the center of a particle is y, as shown in Fig. 3.1, the

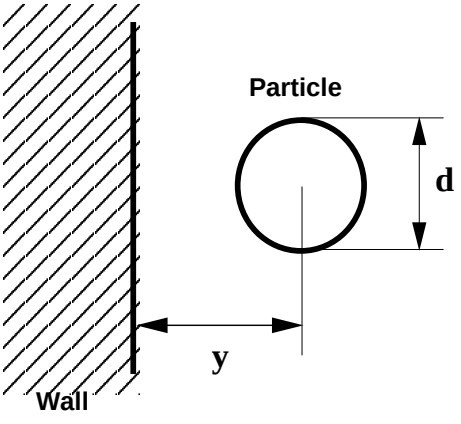

FIGURE 3.1. A particle near a plane wall.

ratio of the actual drag coefficient and the drag coefficient in the case without the wall, C_{w1} and C_{w3}, can be expressed as (Faxén, 1923)

$$C_{w1} = C_{w3} = \left[1 - \frac{9}{16}\eta + \frac{1}{8}\eta^3 - \frac{45}{256}\eta^4 - \frac{1}{16}\eta^5\right]^{-1} . \tag{58}$$

where η is the inverse of distance between the wall and the center of particle, normalized by the particle radius, i.e.

$$\eta = \frac{d}{2y} . \tag{59}$$

O'Neill (1964) found an exact solution for the drag coefficient for a particle moving near a solid wall moving parallel to it by using general bipolar coordinates. The result was in good agreement with the formula by Faxén, Eq. (58), see e.g. Power & Wrobel (1995) for review.

The drag coefficient in the direction normal to the wall is also known to increase near the wall, and several expressions have been proposed. One of them is the approximate solution by Wakiya (1960) derived using the method of reflections, written as

$$C_{w2} = \left[1 - \frac{9}{8}\eta + \frac{1}{2}\eta^3\right]^{-1} . \tag{60}$$

Brenner (1961) solved exactly the governing equations, using bipolar coordinates, and found the wall-normal drag coefficient near a wall as

$$C_{w2} = \frac{4}{3}\sinh\gamma \sum_{n=1}^{\infty} \frac{n(n+1)}{(2n-1)(2n+3)} \times \left[\frac{2\sinh(2n+1)\gamma + (2n+1)\sinh 2\gamma}{4\sinh^2(n+\frac{1}{2})\gamma - (2n+1)^2\sinh^2\gamma} - 1\right] , \tag{61}$$

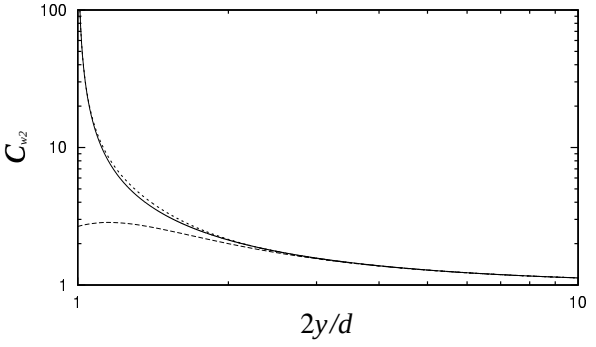

FIGURE 3.2. Drag correction normal to the wall. ——, exact solution by Brenner (1961); — —, approximate solution by Wakiya (1960); - - - -, model in the present study.

where γ is defined by

$$\gamma = \cosh^{-1}\left(\frac{1}{\eta}\right) . \tag{62}$$

Although the expression by Wakiya (1960) is as simple as the expression for C_{w1} by Faxén (1923), it underestimates the correction factor in the vicinity of the wall, say $\eta^{-1} < 2$, as shown in Fig. 3.2. In the vicinity of the wall, the exact solution by Brenner (1961) shows an exponential behavior when η^{-1} approaches 1.

In the present study, C_{w1} and C_{w3}, are computed by the expression by Faxén (1923), i.e. Eq. (58), while C_{w2} is modeled by

$$C_{w2} = \left[\left\{1 - \frac{9}{8}\eta + \frac{1}{2}\eta^3\right\}\left\{1 - e^{-a(1/\eta - b)}\right\}\right]^{-1} \tag{63}$$

This is a combination of the simple expression by Wakiya (1960) and the exponential behavior in the solution of Brenner (1961) and is proposed instead of computing formula (61) directly, in order to save computing time. The constant, b, should be 1 in order to obtain the similar exponential behavior to the exact solution. However, a value very close to but not equal to 1, i.e. $b = 0.9999$ may be used in the simulations to avoid calculations of infinite numbers. The other constant, a, was determined by a least-square fit using 2000 points between $\eta^{-1} = 1$ and $\eta^{-1} = 3$ from the exact solution, resulting in $a = 2.686$.

5.2. Wall surface potential. The wall-surface potential arises due to London-van der Waals force, which is also responsible for surface tension of liquids. According to Chu (1967), the mechanism of generation of wall surface potential is as the following: 1) instantaneous dipoles appear in an atom or a molecule resulting from fluctuations in the electron clouds; 2) dipoles are induced in neighboring atoms or

molecules; 3) global polarization occurs. From the quantum theory, the energy of attraction between two volume elements, dv_1, and dv_2, is calculated as

$$d\Phi = -\frac{Q\ dv_1\ dv_2}{r^6}\ , \tag{64}$$

where Q is a constant which has a dimension of energy.

When the center of a spherical particle with a diameter d is located at a distance of y from a flat wall, similarly to the situation in the previous section, Eq. (64) is integrated over all the volume and reads (e.g. Friedlander, 1977)

$$\Phi = -\frac{\pi^2 Q}{12}\left(\frac{1}{\xi} + \frac{1}{1+\xi} + 2\ln\frac{\xi}{1+\xi}\right)\ , \tag{65}$$

where

$$\xi = \frac{y - d/2}{d} = 2(\eta^{-1} - 1)^{-1}\ . \tag{66}$$

In the $\xi \to 0$ limit, Eq (65) reduces to read

$$\Phi = -\frac{\pi^2 Q}{12\ \xi}\ . \tag{67}$$

In the present study, the wall surface potential is modeled as the boundary condition for particle velocity, similarly to the treatment in Li & Ahmadi (1994), because the effective length of the wall potential, $\sim$ Å, from the wall, is far shorter than the fluid dynamical length scale, $\sim$ μm. The wall-normal velocity of the particle after the impact at the wall, $u_2^{p(after)}$, is given as

$$u_2^{p(after)} = -\mathrm{sgn}(u_2^p)\ \times\ r\sqrt{(u_2^p)^2 - V_c^2}\ , \tag{68}$$

where r is the coefficient of restitution, u_2^p is the particle velocity before the impact. The critical velocity, V_c, is calculated from Eq. (67) as

$$V_c = \sqrt{\frac{2\Phi(y_0)}{m}} \tag{69}$$

where

$$\Phi(y_0) = \frac{\pi^2\ Q\ d}{12\ y_0}\ , \tag{70}$$

The minimum separation length, y_0, can typically be taken as 4 Å(Dahneke, 1972). When the particle velocity is less than V_c, the particle is treated to be deposited on the wall.

The constant, $\pi^2\ Q$, is known as Hamaker constant, A, (Hamaker, 1937). For most of materials, A is of order of 10^{-20}J. The Hamaker constant between two different materials, M1 and M2, can be calculated from the Hamaker constant for these two materials, A_{M1} and A_{M2}, as (Boeheme et al.,1969),

$$A = \sqrt{A_{M1}\ A_{M2}}\ . \tag{71}$$

CHAPTER 4

The model for coupling

1. Forward coupling from fluid to particles

1.1. Filtered scale. The forward coupling is achieved without any special care by computing the particle equation of motion, introduced in the previous chapter. The fluid velocity appearing in the particle equation of motion is computed by a interpolation from grids to particle location. Details about the interpolation will be discussed in the next chapter.

1.2. Subgrid scale fluctuations. One possible model to take into account the influence of SGS fluid velocity on the particle motion is to add an extra term, similarly to the model for the Brownian force, see Eq. (52), such as

$$\frac{f_i^{(SGS)}}{m} = G_i \, \frac{\sigma_S}{\Delta t} \, . \tag{72}$$

Here, σ_S is the increase of standard deviation of particle velocity due to SGS velocity during time Δt.

Following the kinetic theory for particle dispersion in isotropic turbulence (Reeks, 1991), the increase of variance of particle velocity in time Δt can be written, for example in x_2 direction, as

$$\begin{aligned} \sigma_S^2 &= \frac{1}{\tau_p} \int_0^{\Delta t} < u_2^f(0) \, u_2^f(t') > \exp\left(-\frac{t'}{\tau_p}\right) dt' \\ &\quad + \frac{1}{\tau_p} \exp\left(-\frac{2\Delta t}{\tau_p}\right) \int_0^{\Delta t} < u_2^f(0) \, u_2^f(t') > \exp\left(\frac{t'}{\tau_p}\right) dt' \, , \end{aligned} \tag{73}$$

The term, $< u_2^f(0) \, u_2^f(t') >$, is the Lagrangian correlation along particle path and can be modeled (Swailes and Reeks, 1994) as

$$< u_2^f(0) \, u_2^f(t') > = (u')^2 \exp\left(-\frac{t'}{T_{fp}}\right) \, , \tag{74}$$

where u' is the RMS velocity of the fluid, T_{fp} is the integral time scale of fluid velocity along a particle trajectory.

For the present estimate, u' and T_{fp} can be taken as the representative SGS velocity, u_S, and its integral time scale along particle path, T_{Sfp}. The increase of

variance of particle velocity due to SGS velocity in time Δt can then be modeled using Eq. (73) and Eq. (74) as

$$\frac{\sigma_S^2}{(u_S)^2} = \frac{1}{1+\beta}\left[1 - e^{-\alpha(1+\beta)}\right] - \frac{1}{1-\beta}\, e^{-2\alpha}\left[1 - e^{\alpha(1-\beta)}\right] \ , \tag{75}$$

where α and β are defined as

$$\begin{cases} \alpha &= \dfrac{\Delta t}{\tau_p}, \\ \\ \beta &= \dfrac{\tau_p}{T_{Sfp}} \ . \end{cases} \tag{76}$$

The representative SGS velocity, u_S, in Eq. (75) can be estimated as the following. The present SGS model (Zahrai et al., 1995), as well as the classical SGS model, assumes a fully inertial Kolmogorov spectrum (Kolmogorov, 1941; Oboukhov, 1941),

$$E(k) = Ko\, \varepsilon^{2/3} k^{-5/3} \ , \tag{77}$$

where Ko is the Kolmogorov constant, ε is the dissipation rate and k is the wavenumber. An estimate of the SGS kinetic energy, e_S, in terms of dissipation rate, ε_S, and a representative grid size, Δ, can be obtained by integrating $E(k)$ from $k = \pi/\Delta$ to $k = \infty$. This results in

$$e_S^{3/2} = \frac{1}{c_\varepsilon} \varepsilon_S \Delta \ , \tag{78}$$

where c_ε is defined by

$$c_\varepsilon = \pi \left(\frac{2}{3\ Ko}\right)^{3/2} \ . \tag{79}$$

A standard value of the Kolmogorov constant (see e.g. Lesieur, 1997), $Ko = 1.5$, yields $c_\varepsilon = 0.96$.

By assuming a relation between the SGS energy in cell, e_S, and velocity, u_S, as

$$e_S = \frac{3}{2} u_S^2 \ , \tag{80}$$

and by estimating Δ as the geometric mean of the cell, see Eq. (20), u_S can then be written as

$$u_S = \sqrt{\frac{2}{3}}\, c_\varepsilon^{-1/3} \varepsilon_S^{1/3} (\Delta x_1 \Delta x_2 \Delta x_3)^{1/9} \ . \tag{81}$$

With help of the relation between ε_S, the length scale, ℓ_{Si}, and the SGS viscosity, ν_{Si}, used in the derivation of SGS model, Eq. (30), and the relation between ℓ_S and Δx_i, (see e.g. Canuto and Cheng, 1997),

$$\ell_{Si} = \frac{\Delta x_i}{c_\varepsilon} \ , \tag{82}$$

TABLE 4.1. Estimated influence of SGS fluid velocity for the cases in Paper 3.

d [μm]	0.01	0.1	1	10
σ_B^+	3.62×10^2	3.17	1.58×10^{-2}	5.33×10^{-5}
Near the wall,				
$x_2^+ = 1.45$, $u^{+M} = 0.105$.				
σ_S^+	0.105	0.105	0.105	3.00×10^{-2}
Ratio: σ_S^+/σ_B^+	2.90×10^{-4}	3.31×10^{-2}	6.65	5.62×10^2
Buffer region,				
$x_2^+ = 12$, $u^{+M} = 0.235$.				
σ_S^+	0.235	0.235	0.235	4.62×10^{-2}
Ratio: σ_S^+/σ_B^+	6.49×10^{-4}	7.41×10^{-2}	14.9	8.67×10^2

Eq. (81) becomes

$$\begin{aligned} u_S &= \sqrt{\frac{2}{3}}\, c_\varepsilon^{-1/3} \left(\frac{\nu_{Si}}{(\ell_{Si})^{4/3}} \right) (\Delta x_1 \Delta x_2 \Delta x_3)^{1/9} \\ &= \sqrt{\frac{2}{3}}\, c_\varepsilon^{-1/3} \left(\frac{\nu_{Si}\, c_\varepsilon^{4/3}}{(\Delta x_i)^{4/3}} \right) (\Delta x_1 \Delta x_2 \Delta x_3)^{1/9} \\ &= \sqrt{\frac{2}{3}}\, c_\varepsilon \nu_{Si} (\Delta x_1 \Delta x_2 \Delta x_3)^{1/9} (\Delta x_i)^{-4/3} \ . \end{aligned} \tag{83}$$

Finally by substituting ν_{Si}, see Eq. (32), into Eq. (83), an estimate of u_S in terms of the variables in the resolved scale,

$$u_S = \frac{2}{\sqrt{3}}\, c_\varepsilon\, C_S^2 (\Delta x_1 \Delta x_2 \Delta x_3)^{1/3} |\overline{s_{ij}}| \ , \tag{84}$$

can be obtained.

It is known from numerical simulations (e.g. Huang and Leonard, 1995) that the Lagrangian integral time scale of an isotropic turbulence, T_L, is of the same order of magnitude as the eddy-turnover time, T_0. For particles with relatively small inertia, the Lagrangian integral time scale along the particle path, T_{fp} may also be the same magnitude as T_0. Therefore T_{Sfp} in Eq. (75) for such particles can be estimated by the eddy-turnover time of the SGS eddies, T_{S0}, defined as

$$T_{S0} = \frac{\dfrac{3\pi}{4u_S} \displaystyle\int_{\pi/\Delta}^{\infty} k^{-1} E(k) dk}{\displaystyle\int_{\pi/\Delta}^{\infty} E(k) dk} = \frac{3}{10} \frac{\Delta}{u_S} \ . \tag{85}$$

Substituting the estimate of u_S, Eq (84) into Eq (85), T_{Sfp} can be estimated as a function of resolved deformation rate as

$$T_{Sfp} \simeq T_{S0} = \frac{3\sqrt{3}}{20\, c_\varepsilon\, C^2} \frac{1}{|\overline{s_{ij}}|} \,. \tag{86}$$

Estimated values for particles with very short relaxation time, $\tau_p^+ < 10$, considered in Paper 3, are shown in Table 4.1 According to that, the SGS fluid velocity may have considerable influences on particle motion when τ_p^+ is of order of one. In the cases where the Brownian force is more significant, i.e. for very small particles, or when the particle inertia is large, say $\tau_p^+ > 10$, the influence of SGS fluid velocity can be neglected. Note that a similar estimate is done in Paper 3, using a different estimate of time scale, i.e.

$$T_{S0} = \frac{1}{|\overline{\omega_i}|} \,, \tag{87}$$

where ω_i is the vorticity, and the same conclusion is drawn.

2. Backward coupling from particles to fluid

2.1. Filtered scale. Influence of presence of particles on the fluid motion has not yet been fully understood. In some cases, e.g. bubble flow, the presence of particle may produce velocity fluctuations of the surrounding fluid whose wavelength is smaller than the particle diameter (Esmaeeli & Tryggvason, 1998).

However, it was numerically shown by Pan & Banerjee (1996) that the particles works as if they were extra burden to the fluid when the particles are small and have much larger density than surrounding fluid, as is the case in the present study. In such case, the momentum transfer from particles to fluid can successfully modeled by adding the reaction force against the surface force acting on the particle to the Navier-Stokes equation. This model is sometimes referred to as force coupling model or particle-source-in-cell (PSI-CELL) model (Crowe et al., 1977) in contrast to the velocity coupling model (Pan & Banerjee, 1996) in which the velocity disturbance around the particle is considered.

2.2. Influence of particles on SGS model. When two-way coupling is modeled by the force coupling model, as mentioned above, an extra term appears in the transport equation of the subgrid energy of fluid, Eq. (10), i.e.

$$\frac{\partial e_S}{\partial t} + \overline{u_j^f} \frac{\partial e_S}{\partial x_j} = \mathcal{P}_S - \frac{\partial}{\partial x_j} J_{Sj} - \varepsilon_S + \overline{u_k^{f\prime} f_k'} \,, \tag{88}$$

where f_i' is the fluctuation component of the force from particles to fluid.

The last term can be modeled as

$$\overline{u_k^{f\prime} f_k'} = S\alpha^p \overline{(\overline{\beta} + \beta')(u_k^{f\prime} u_k^{p\prime} - u_k^{f\prime} u_k^{f\prime})} \,, \tag{89}$$

where $S = \rho^p/\rho^f$ and α^p is the volume fraction in the cell occupied by the particles. When the particle Reynolds number is not much larger than unity and the fluctuation of the drag coefficient can be negligibly small, Eq. (89) is simplified to read

$$\overline{u_k^{f\prime} f_k'} = S\alpha^p B(\overline{u_k^{f\prime} u_k^{p\prime}} - \overline{u_k^{f\prime} u_k^{f\prime}}) \ , \tag{90}$$

where

$$B = \overline{\beta} \simeq \tau_p^{-1} \ . \tag{91}$$

Although several formulae have been proposed for the approximation of $\overline{u_k^{f\prime} u_k^{p\prime}}$, the model by Porahmadi & Humphrey (1983) and Gavin et al. (1983)

$$\overline{u_k^{f\prime} u_k^{p\prime}} = 2e_S \left[1 + \frac{1}{B\tau_e}\right]^{-1} \tag{92}$$

is adopted here for simplicity. Here, τ_e is the time scale of the energetic eddies in the original model. In the subgrid scale model, τ_e may be taken as the eddy-turnover time, T_{S0}, see Eq. (85). Using these models, Eq. (89) can be expressed, after simple algebra, as

$$-\overline{u_k^{f\prime} f_k'} = S\alpha^p B \frac{15u_S^3}{3B\Delta + 10u_S} \ . \tag{93}$$

Substituting Eq. (81) into u_S on the numerator and Eq. (84) into u_S on the denominator, one finally obtains

$$-\overline{u_k^{f\prime} f_k'} = \frac{10\sqrt{6}}{9\ c_\varepsilon} \frac{S\alpha^p}{1+\eta_B} \varepsilon_S \ , \tag{94}$$

where η_B is the ratio of particle time scale to eddy-turnover time,

$$\eta_B = \frac{\tau_p}{T_{S0}} = \frac{20\ c_\varepsilon\ C_S^2}{3\sqrt{3}} \frac{|\overline{s_{ij}}|}{B} \ . \tag{95}$$

The subgrid scale viscosity, ν_{Sp}, can then be estimated, following the derivation of the SGS model by Zahrai et al. (1995), see Eq. (30), as

$$\begin{aligned} \nu_{Sj} &= (\varepsilon_S - \overline{u_k^{f\prime} f_k'})^{1/3}\ \ell_{Sj}^{4/3} \\ &= \varepsilon_S^{1/3} \ell_{Sj}^{4/3} \left(1 + \frac{10\sqrt{6}}{9\ c_\varepsilon} \frac{S\alpha^p}{1+\eta_B}\right)^{1/3} \\ &= \nu_{Sj}^0 \left(1 + \frac{10\sqrt{6}}{9\ c_\varepsilon} \frac{S\alpha^p}{1+\eta_B}\right)^{1/3} \ . \end{aligned} \tag{96}$$

where ν_{Sj}^0 is the subgrid scale viscosity in the case of the unladen flow. As can be noticed, ν_{Sj} is the function of the local mass fraction, $S\alpha^p$, and the ratio of time scales, η_B.

TABLE 4.2. Estimated error in SGS model due to presence of particles. Around $y^+ = 12$ plane.

Case (Paper No.)	50 μm glass (5)	70 μm copper (5)	70 μm copper (7)
Re_τ	180	180	644
$S\alpha^p$	0.60	4.4	3.2×10^{-2}
η_B	5.9	41	1.0×10^{2}
Error: $(\nu_{Sj} - \nu^0_{Sj})/\nu^0_{Sj}$	7.1×10^{-2}	8.5×10^{-2}	2.8×10^{-4}

The change of subgrid scale viscosity due to the presence of particles can be estimated for the cases in the present study. The estimated values around $y^+ = 12$ for some cases are presented in Table 4.2. According to the table, the estimated error in SGS model due to the presence of particles is 7-9% in the cases presented in Paper 5, and negligibly small in the case in Paper 7.

The estimate above may not be accurate if the energy spectrum in the subgrid scale is largely modified by the presence of particles such that the assumption of the inertial energy cascade is no more valid or length scale, ℓ_{Sj}, is largely changed. However, an accurate estimation may only be achieved by an analysis of the data computed from fully DNS which can resolve up to the smallest eddies around the particle-fluid boundaries.

3. Inter-particle collisions

When the number density of the particle and the collision frequency are sufficiently large, inter-particle collisions can be modeled as a stochastic model (Yonemura et al., 1993; Sommerfeld, 1999). The collisions are computed by probability, in a way similar to direct simulation Monte Carlo (DSMC) method for simulations of molecules.

On the other hand, when the number density of the particles is small, inter-particle collisions can be computed directly by judging the occurrence of collisions from particle trajectories and computing the velocity changes according the momentum and energy conservation laws (Tanaka & Tsuji, 1991). In the present study, the latter one, i.e. the direct approach, is adopted.

The inter-particle collisions are computed according to the following procedures. At first, provisional positions of the particles at time $(t + \Delta t)$ are computed without taking into account collisions, as represented by dotted circles in Fig. 4.1. For the judgement whether collisions occur between two neighbouring particles, the method described by Yamamoto et al. (1998) can be used. Namely, two particles, labeled as Particle 1 and Particle 2 as shown in Fig 4.1, can be judged to collide if

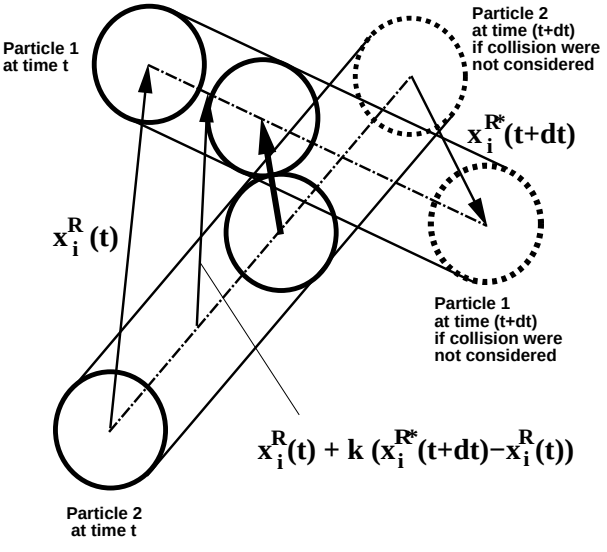

FIGURE 4.1. Inter-particle collision.

the equation about the distance between their trajectories,

$$|\vec{x}^R(t) + k(\vec{x}^{R*}(t+\Delta t) - \vec{x}^R(t))|^2 = d^2 \ , \tag{97}$$

has two real roots, k_1 and k_2 $(k_1 \leq k_2)$, and the value of smaller real root, k_1, is between 0 and 1, i.e. $0 \leq k_1 \leq 1$. Here, $\vec{x}^R(t)$ is the position of Particle 1 relative to Particle 2 at time t, i.e.

$$x_i^R(t) = x_i^{(1)}(t) - x_i^{(2)}(t) \ , \tag{98}$$

and $\vec{x}^{R*}(t+\Delta t)$ is the provisional position of Particle 1 relative to Particle 2 at time $(t+\Delta t)$. If these particles are judged to collide, the normal unit vector from the center of Particle 2 to the center of Particle 1 at the contact, $\vec{n}^R$, can be computed as

$$n_i^R = \frac{1}{d}\{x_i^R(t) + k_1(x_i^{R*}(t+\Delta t) - x_i^R(t))\} \ . \tag{99}$$

By assumming here a perfectly elastic collision, the velocities of Particle 1 and Particle 2 after the collision, $u_i^{(1,\,after)}$ and $u_i^{(2,\,after)}$, can be computed by

$$\begin{cases} u_i^{p(1,\,after)} &= u_i^{p(1)}(t) - u_j^R(t)\, n_j^R n_i^R \ , \\ u_i^{p(2,\,after)} &= u_i^{p(2)}(t) + u_j^R(t)\, n_j^R n_i^R \ , \end{cases} \tag{100}$$

where $u_i^R(t)$ is the relative velocity,

$$u_i^R(t) = u_i^{(1)}(t) - u_i^{(2)}(t) \ . \tag{101}$$

Finally, the correct positions of these particles at time $(t + \Delta t)$ can be computed by

$$\begin{cases} x_i^{p(1)}(t+\Delta t) &= u_i^{p(1)}(t)\, k_1 \Delta t + u_i^{p(1,\, after)}\, (1-k_1)\Delta t\ , \\ x_i^{p(2)}(t+\Delta t) &= u_i^{p(2)}(t)\, k_1 \Delta t + u_i^{p(2,\, after)}\, (1-k_1)\Delta t\ . \end{cases} \tag{102}$$

CHAPTER 5

Numerical procedure

1. Overview

The filtered Navier-Stokes equation, Eq. (7), is integrated in the same way as the SMAC method (Amsden & Harlow, 1970). A difference from the original SMAC method is that the integration is done using a third order Adams-Bashforth scheme, i.e.

$$\overline{u_i^f}^{n+1} = \overline{u_i^f}^{n} + \Delta t \left[\frac{23}{12}\phi_i^n - \frac{16}{12}\phi_i^{n-1} + \frac{5}{12}\phi_i^{n-2} \right] , \tag{103}$$

where ϕ_i represents the right hand side of Eq. (7) and the superscripts, $n+1$, n, $n-1$ and $n-2$, denote the time steps. The Poisson equation for the pressure is accordingly modified to satisfy the continuity equation, Eq. (1). The advection and diffusion terms are discretized on a staggered mesh system using the second-order central difference scheme.

After that instantaneous fluid velocities are computed on the staggered mesh, they are interpolated to the particle locations for the integration of particle equation of motion. Details on the interpolation schemes and their accuracy is discussed in the next section.

The particle equation of motion, Eq. (39), is also integrated with the third order Adams-Bashforth scheme for most of the cases. Exception is the case when very small particles are considered (Paper 3). In that case, the particle equation of motion is discretized using the implicit Euler method in order to avoid numerical instabilities that can occur due to extremely small particle relaxation time, τ_p.

The computational time step used in the integration is $\Delta t^+ = 0.18$, in wall unit, for the flow at $Re_\tau = 180$ and $\Delta t^+ = 0.322$ for $Re_\tau = 644$. The same time step is used for the integration of the particle equation of motion.

One computation for dilute flow with about 2000 particles, for instance, such as the cases presented in the Paper 6 and Paper 7, takes about two CPU days from the initial state to its convergence (about 20000 time steps) and one more CPU day to accumulate statistics (about 10000 time steps) on DEC AlphaServer 4100 5/466. The computation time, of course, increases with the number of particles. For the cases presented in Paper 3, with 360000 particles, it takes two CPU weeks

for one case, from the initial state to the end of the simulation (about 20000 time steps) on the same machine.

2. Accumulation of statistics

Various kinds of statistics such as first order and second order moments, i.e. mean and RMS values, and probability density function (PDF) are computed, based on both volume average and particle ensemble average. The statistics of interest for each case are presented in the corresponding paper.

The statistics are often presented in wall units, denoted by a superscript, $+$. For physical values of velocity u, length x, and time t, the nondimensional values in wall units, u^+, x^+ and t^+, are defined, respectively, as

$$\begin{cases} u^+ = \dfrac{u}{u_\tau} , \\ x^+ = \dfrac{x\, u_\tau}{\nu} , \\ t^+ = \dfrac{t\, u_\tau^2}{\nu} , \end{cases} \tag{104}$$

where u_τ is the shear velocity, ν is the kinematic viscosity of the fluid. When the superscript, $+$, is used for the particle number density in the present study, it means the particle number density normalized with the initial particle number density.

In the presentation of statistics, the velocity components, u_1, u_2 and u_3, and are often denoted as u, v and w. Similarly, x_1, x_2 and x_3 are expressed as x, y and z.

In the simulations for Paper 4 - Paper 7, different terms in various balance equations in Eulerian frame are examined using the computed statistics, similarly to those presented in Paper 4. The balance of different terms is not presented in Paper 5 - Paper 7, though, that is used to judge whether the flow is fully developed.

Here, for example, such balance in the case of one-way coupling simulation of 70 μm copper particles in a turbulent channel flow at $Re_\tau = 644$, i.e. Case 1a in Paper 6, is examined. Starting from the balance equations based on particle ensemble average (Simonin, 1996), the balance equations for momentum, kinetic stress tensor, mean kinetic energy and fluctuating kinetic energy can reduce for the case of channel flow to read:

- Momentum balance

$$\left(N \frac{\partial U_i}{\partial t} = \right) \quad 0 = -\frac{\partial}{\partial x_2} \left(N < u_2 u_i > \right) + N g_i + N F_i \ , \tag{105}$$

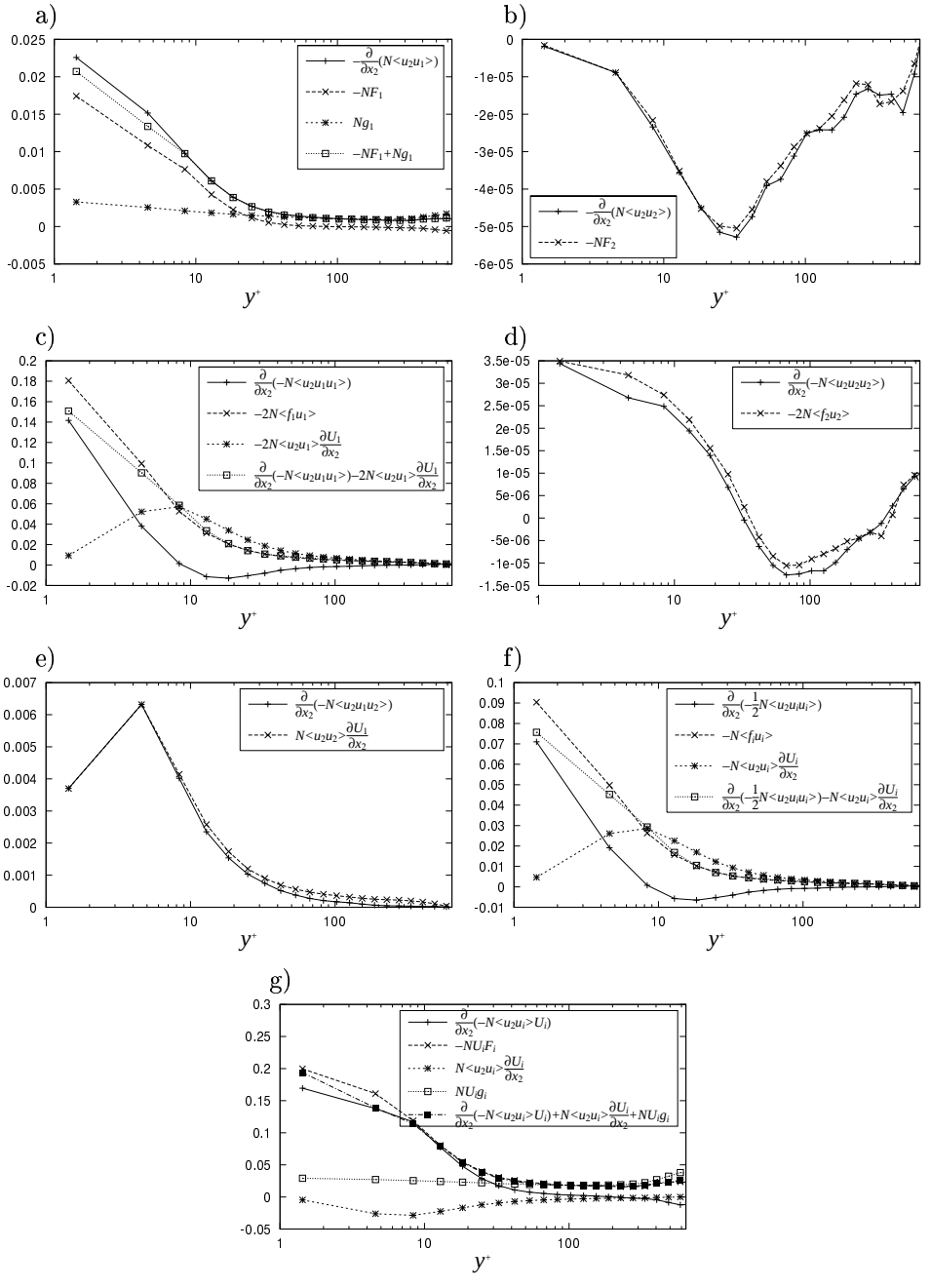

FIGURE 5.1. Various balances in one-way coupling simulation of 70 μm copper particles in a channel flow at $Re_\tau = 644$ (Case 1a, Paper 6). Corresponding to the balance equation for: a) U_1; b) U_2; c) $< u_1u_1 >$; d) $< u_2u_2 >$; e) $< u_1u_2 >$; f) $\frac{1}{2} < u_iu_i >$; g) $\frac{1}{2}U_iU_i$.

- Kinetic stress tensor balance

$$\left(N\frac{\partial < u_iu_j >}{\partial t} =\right) \quad 0 \quad = \quad -\frac{\partial}{\partial x_2}\left(N < u_2u_iu_j >\right)$$
$$-N\left(< u_2u_i > \frac{\partial U_j}{\partial x_2} + < u_2u_j > \frac{\partial U_i}{\partial x_2}\right) \tag{106}$$
$$+N\left(< f_iu_j > + < f_ju_i >\right) \ ,$$

- Mean kinetic energy balance

$$\left(N\frac{\partial(\frac{1}{2}U_iU_i)}{\partial t} =\right) \quad 0 \quad = \quad -\frac{\partial}{\partial x_2}\left(N < u_2u_i > U_i\right) + N < u_2u_i > \frac{\partial U_i}{\partial x_2}$$
$$+NU_ig_i + NU_iF_i \ , \tag{107}$$

- Fluctuating kinetic energy balance

$$\left(N\frac{\partial(\frac{1}{2}u_iu_i)}{\partial t} =\right) \quad 0 \quad = \quad \frac{\partial}{\partial x_2}\left(\frac{1}{2}N < u_2u_iu_i >\right) - N < u_2u_i > \frac{\partial U_i}{\partial x_2}$$
$$+N < f_iu_i > \ . \tag{108}$$

Here, the superscripts representing particle variables, p, and wall unit, $+$, are dropped for simplicity in notation. N represents the number density, U_i is the mean particle velocity, F_i is the mean force from fluid per unit mass. The variables in lower case represent the fluctuating parts. Profiles of each term in these equations are shown in Fig.5.1a-g.

It might be more interesting to show similar balances for the cases including inter-particle collisions, e.g. cases in Paper 7. For the mean and fluctuating kinetic energy balances, where the inter-particle collision term resulted in zero due to the model of perfectly elastic collision, similar curves to Fig.5.1f-g are obtained. For the other balances, however, smooth curves cannot be drawn due to insufficient sample size.

3. Accuracy of different interpolation schemes

In order to integrate the particle equation of motion, different quantities of fluid computed on the mesh have to be interpolated to the positions of the particles. A linear interpolation is used in Paper 2, Paper 4 and Paper 5. In Paper 4, a nearest grid point (NGP) interpolation and a sixth order Lagrangian interpolation are also tested. In more recent papers, i.e. Paper 1, Paper 3, Paper 6 and Paper 7, a fourth order Lagrangian interpolation is used. In all cases, a bisection method is used in order to relate the locations of particles and mesh.

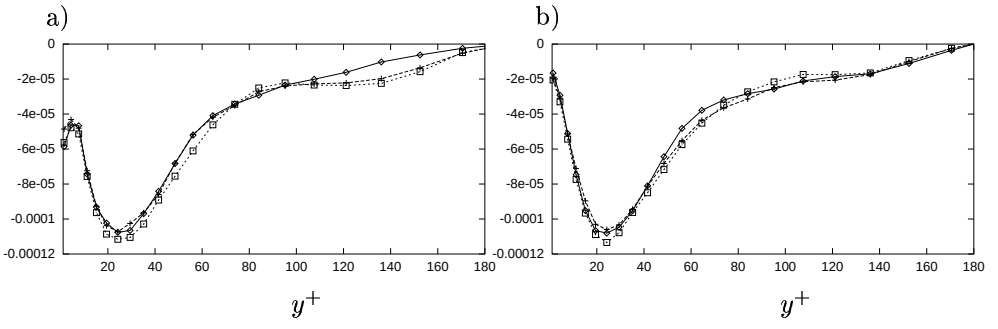

FIGURE 5.2. Major terms in the y-direction particle momentum balance equation, Eq. (19) in Paper 4, based on the statistics 70 μm copper particles of accumulated during $6 < t\ u_\tau/\delta < 12$. a) turbulent transport term, $-\dfrac{d}{dy^+}N^+ < v^{+p}v^{+p} >^p$; b) mean drag force, F_y^+. —◇—, NGP; - - -+- - -, linear, - - -□- - -, 6th-order Lagrangian.

When the particle is located at (x^p, y^p, z^p) in a cell whose vertices are (x_0, y_0, z_0) ... (x_1, y_1, z_1), the n-th order Lagrangian interpolation can be expressed as

$$u^f(x^p,y^p,z^p) = \sum_{i=1-\frac{n}{2}}^{\frac{n}{2}} \sum_{j=1-\frac{n}{2}}^{\frac{n}{2}} \sum_{k=1-\frac{n}{2}}^{\frac{n}{2}} \left(\prod_{\substack{l=1-\frac{n}{2} \\ (l\neq i)}}^{\frac{n}{2}} \frac{x^p-x_l}{x_i-x_l} \cdot \prod_{\substack{l=1-\frac{n}{2} \\ (l\neq j)}}^{\frac{n}{2}} \frac{y^p-x_l}{y_j-x_l} \prod_{\substack{l=1-\frac{n}{2} \\ (l\neq k)}}^{\frac{n}{2}} \frac{z^p-x_l}{z_k-x_l} \right) u^f_{ijk} \ , \tag{109}$$

where the subscripts i, j, k and l represent the cell indexes, different from those used in the previous chapters. The linear interpolation corresponds to a second order Lagrangian interpolation.

Evaluation of accuracy of interpolation schemes has been reported by several researchers. Balachander & Maxey (1989) tested different interpolation schemes for

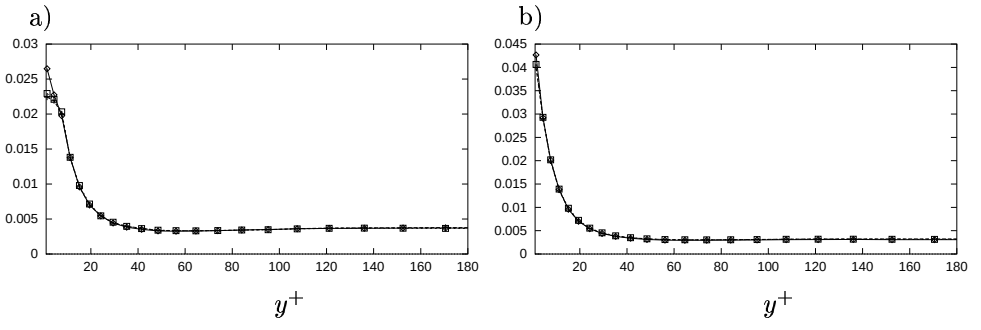

FIGURE 5.3. Major terms in the x-direction particle momentum balance equation, Eq. (19) in Paper 4, based on the statistics 70 μm copper particles of accumulated during $6 < t\ u_\tau/\delta < 12$. a) gravitational force + turbulent transport, $N^+g^+ - \dfrac{d}{dy^+} < u^{+p}v^{+p} >^p$; b) mean drag force, F_x^+. —◇—, NGP; - - -+- - -, linear, - - -□- - -, 6th-order Lagrangian.

homogeneous turbulence generated by spectral simulation, and found that the statistics of fluid were retained with a good accuracy when the Hermite interpolation, the sixth order Lagrangian interpolation or the so-called TS13 scheme proposed by Yeung & Pope (1988) were used; while the linear interpolation generated large error as compared to statistics in the original field.

Accuracy of different interpolation schemes in a frozen turbulent channel flow was studied by Wang & Squires (1996b). Similarly to the analysis by Balachander & Maxey (1989), they found that the statistics of fluid were retained when the sixth-order and the fourth-order Lagrangian interpolation schemes were used; while large errors were found in the second order momentum when the linear interpolation was used.

As an extension of the study by Wang & Squires (1996b), influences of the different interpolation schemes on the statistics of particles with large inertia are investigated. Different from the analysis by Wang & Squires, investigation is done for the long term statistics of particles. The same systems as those presented in Paper 4, i.e. 50 μm glass and 70 μm copper particles in a flow at $Re_\tau = 180$, are simulated with different interpolation schemes: 1) NGP, 2) linear, 3) sixth order Lagrangian. It can be found that the particle statistics, which are the main output of the simulations, such as mean and RMS values of particle velocity, shown in Fig. 3 of Paper 4, and terms in the balance equation, Figs. 5.2 and 5.3, are not largely influenced by the differences in interpolation scheme. This can be due to

insensitivity of such particles with large inertia to the small scale turbulence which is filtered out by lower order interpolation.

4. Validation of LES

Validation of the LES with an anisotropic subgrid model used in the present study, has been done in the previous work by Zahrai et al. (1995). A turbulent channel flow at $Re_\tau = 180$, which is the same value as the direct numerical simulation by Kim et al. (1987), was taken as a test case. The computational domain was also set the same as that in Kim et al. (1987), i.e. $4\pi\delta$, 2δ and $2\pi\delta$ in the streamwise (x), wall-normal (y) and the spanwise (z) directions, respectively. Zahrai et al. (1995) performed several numerical experiments for a turbulent channel flow at $Re_\tau = 180$ using different number of mesh, $N_x \times N_y \times N_z$, corresponding to different mesh sizes, Δx^+, Δy^+ and Δz^+, as shown in Table 5.1, and model constants, C, of 0.08 and 0.12, and found reasonable agreement with DNS data up to third order moments in Case 1 and Case 2 with $C = 0.08$. The summary of their results are shown in Table 5.2. The maximum value of RMS level of the streamwise velocity, Max (u'), the position where Max (u') appears, Y^+, the mean separation of streaks near the wall, Y^+, mean velocity, U_m, and the ratio of centerline velocity and mean velocity, U_C, in Case 1 and Case 2 are again in good agreement with the DNS data by Kim et al. (1987).

Validation for the case at a higher Reynolds number, $Re_\tau = 644$, is presented in Paper 7. A good agreement is found between the data computed using the present LES with and experimental data by Kulick et al. (1994).

TABLE 5.1. Specification of mesh spacings (Zahrai et al., 1995).

	Kim et al.	Case 1	Case 2	Case 3	Case 4	Case 5	Case 6
N_x	192	32	32	32	32	24	32
N_y	129	42	42	42	32	32	32
N_z	160	128	96	64	48	48	36
Δx^+	12	70.7	70.7	70.7	70.7	94.25	70.7
Δz^+	7	8.8	11.8	17.7	23.6	23.6	31.4
Δy^+_{min}	0.05	2.8	2.8	2.8	5.0	5.0	5.0
Δy^+_{max}	4.4	18.9	18.9	18.9	20.9	20.9	20.9

TABLE 5.2. Summary of the results of the large eddy simulations (Zahrai et al., 1995).

	Kim et al.	Case 1	Case 2	Case 3	Case 4	Case 5	Case 6
Max (u')	2.7	2.85	2.90	2.92	3.04	3.1	3.1
Y^+	12	15.8	15.8	16.1	17.2	18.1	23.4
Λ^+	100	114	120	122	124	124	160
U_m	15.63	15.2	15.2	15.5	15.8	15.8	17.2
U_C/U_m	1.16	1.13	1.14	1.15	1.16	1.16	1.17

CHAPTER 6

Summary of papers

Paper 1

A passive scalar transport in a turbulent channel flow is simulated using LES. Different Schmidt numbers equal to 1, 10 and 100 are used for the passive scalar. The governing equation for fluid and that for passive scalar are discretized on different mesh of different sizes, such that larger and geometry dependent structure of each field can be captured. The velocity on the mesh for passive scalar field was obtained by interpolating from the mesh for fluid velocity field, using the a fourth-order Lagrangian interpolation.

The methodology is validated through comparisons with documented data from earlier large eddy and direct numerical simulations. Moreover, influence of typical boundary conditions appearing in electrochemical problem on the statistics is studied.

Paper 2

The methodology of Lagrangian particle tracking coupled with LES (LPT-LES) is validated.

Similarly to the LPT-DNS by Rouson & Eaton (1994) and the LPT-LES by Wang & Squires (1996b), turbulent channel flows of air at $Re_\tau = 180$ with 50 μm glass particles ($\tau_p^+ = 117$) and 70 μm copper particles ($\tau_p^+ = 810$) are simulated. Drag force and the gravitational force are included in the particle equation of motion. One-way coupling is assumed.

Excellent agreement is found between simulation data of the present study, Rouson & Eaton (1994) and Wang & Squires (1996b) both in the mean particle velocity profile and the velocity fluctuations. Development time of the flow and sample size are also discussed on using the simulation data.

Paper 3

Turbulent channel flows of air at $Re_\tau = 180$ with small graphite particles with diameter of 0.01 - 10 μm ($\tau_p^+ = 9.79 \times 10^{-5} - 4.51$; $Sc = 2.87 \times 10^2 - 6.22 \times 10^6$) are simulated using LPT-LES. In addition to drag force and gravitational force, Brownian force and Saffman lift force are taken into account in the particle equation of motion. One-way coupling is assumed.

Relation between the relaxation time, and the deposition velocity of small particles in a turbulent channel is studied, and a good agreement with an empirical relation suggested by Wood (1981) and simulation results by Li & Ahmadi (1993) are found. The relative importance and the correlations of different forces are discussed using the statistics obtained in the simulations. The influences of the dynamics of turbulent structure near the wall is also investigated using a simple model.

Paper 4

As a continuation from Paper 2, statistics of 70 μm copper particles and 50 μm glass particles in a turbulent channel flow are computed using LPT-LES.

The statistics of particles are compared with the data presented in Paper 2 and in Wang & Squires (1996b) which used a shorter development time. Both in the cases of 70 μm copper particles and 50 μm glass particles, slight decrease of the mean particle velocity and slight increase of the particle number density are observed near the wall.

The statistics are used for a detail study of force balance in Eulerian frame. Based on the investigations on the force balance, simplified versions of averaged momentum equations for particle phase are presented.

(Erratum for paper 4)

The prefactor for the history term in Eq. (1) should read

$$\frac{9\nu}{d\,S}\,.$$

Paper 5

Two-way coupling LPT-LES is performed for cases with the same parameters considered in Paper 4. The computed statistics are compared with those from the one-way coupling simulations presented in Paper 4.

The presence of 50 μm glass particles at mass flow rate of 0.4 is found to suppress the transverse RMS velocity components and the Reynolds stress in the whole channel. The streaky structure of near-wall turbulence is also found to be modulated. For 70 μm copper particles at mass flow rate of 3.0, the turbulent structure is found to totally be destroyed.

A relation between the fluid stresses and the inter-phase stress are derived, and are validated using the simulation data.

(Appendix for Paper 5)

As pointed out by Liné[1], there is some inconsistency in the values of friction velocity,

[1]Liné, A., 1997. As a reviewer at the Licentiate seminar of the author, KTH, Stockholm, Sweden, 6 June 1997.

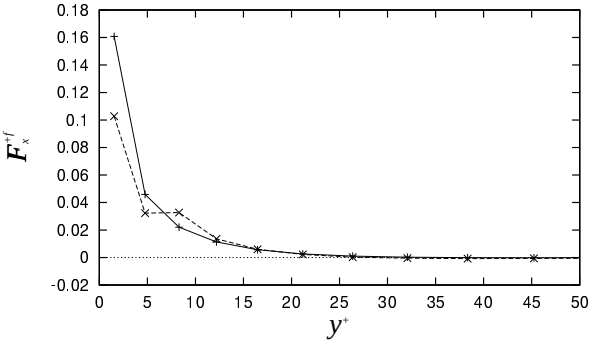

FIGURE 6.1. Momentum balance of particles. —+—, momentum gain due to gravity, plus turbulent transport; - - -×- - -, momentum transfer to fluid.

u_τ, computed using Eq. (16) in Paper 5,

$$u_\tau^2 = -\frac{\delta}{\rho^f}\frac{dP_0}{dx} + \frac{1}{\rho^f}\int_0^\delta F_x^f\, dy \ . \tag{110}$$

If the flow is fully developed, the total momentum from particles to fluid, $\int_0^\delta F_x^f\, dy$, should be balanced with the momentum which particles gains from the gravitational force, as pointed out by Portela[2]. Since the pressure gradient is set to be a constant in the simulation, such that

$$-\frac{1}{\rho^f}\frac{dP}{dx} = \frac{u_{\tau 0}^2}{\delta} \ , \tag{111}$$

where $u_{\tau 0}$ is the friction velocity of the undisturbed flow, Eq. (110) can be rewritten as

$$u_\tau^2 = u_{\tau 0}^2 + \delta S\alpha^0 g \ . \tag{112}$$

In the case of 50 μm glass particles studied in the paper, the half channel width, δ, is 9.00×10^{-3} m, the mass fraction, $S\alpha^0$, is 0.300, the gravity, g, is 9.80 m^2/s, and $u_{\tau 0} = 0.300$ m/s. Substituting these values into Eq. (112), one obtains $u_\tau = 0.341$. The Reynolds number is then computed as $Re_\tau = 205$.

On the other hand, the values shown in Table 2 are ones calculated using the computed statistics. Fig. 6.1 shows the magnitude of momentum transfer from particles to fluid, F_x^{+f}, normalized by the friction velocity of the undisturbed flow

[2]Portela, L, 1998. Private communication at the 3rd Int. Conf. Multiphase Flow, Lyon, France, 8-12 June 1998.

and the bulk mass ratio. Using F_x^{+f}, Eq. (110) reads

$$\begin{aligned} u_\tau^2 &= u_{\tau 0}^2 + \frac{1}{\rho^f}\int_0^\delta F_x^f dy \\ &= u_{\tau 0}^2 + S\alpha^0 u_{\tau 0}^2 \int_0^{\delta^+} F_x^{+f} dy^+ \end{aligned} \quad . \tag{113}$$

The total momentum transfer in wall unit, $\int_0^{\delta^+} F_x^{+f} dy^+$, can be computed as 0.609. The friction velocity can be calculated as $u_\tau = 0.326$ and the Reynolds number is $Re_\tau = 196$.

Reason for the discrepancy may be that development of the flow was still insufficient concerning to the balance of the streamwise momentum, as seen in Fig. 6.1.

Paper 6

In this paper, the influences of inter-particle collision and the drag correction factor near the wall are investigated by performing LPT-LES with or without these effects.

Similarly to the experiment by Kulick et al. (1994), a turbulent channel flow of air at $Re_\tau = 644$ with 70 μm copper particles ($\tau_p^+ = 2000$) is considered. Mass loading is set at 2%.

Inter-particle collisions are found to be of crucial importance even at 2% mass loading, while the effect of two-way coupling on the statistics is too small to be visible. The drag correction near the wall is found also to be important when the inter-particle collisions are taken into account.

(Errata for paper 6)

The drag correction by Wakiya (1960), Eq. (5), should read

$$C_{wy} = \left[1 - \frac{9}{8}\left(\frac{d^+}{2y^+}\right) + \frac{1}{2}\left(\frac{d^+}{2y^+}\right)^3\right]^{-1}$$

and also the model formula, Eq. (7), should read

$$C_{wy} = \left[\left\{1 - \frac{9}{8}\left(\frac{d^+}{2y^+}\right) + \frac{1}{2}\left(\frac{d^+}{2y^+}\right)^3\right\}\left\{1 - \exp\left(-a\left(\frac{2y^+}{d^+} - b\right)\right)\right\}\right]^{-1} \quad .$$

Paper 7

As a continuation from Paper 6, a gas-particle turbulent channel flow at $Re_\tau = 644$, loaded with 70 μm copper particles is simulated using LPT-LES. Inter-particle collisions and the increase of drag coefficient near the wall are taken into account. Different particle-wall boundary conditions are examined.

The agreement with the experimental data by Kulick et al. (1994) is found to be significantly improved when a particle-wall boundary condition, that can suppress a direct re-entrainment of particles after an impact at the wall, is used.

Using the statistics computed with such a boundary condition, mechanism of occurence of the bimodal streamwise velocity distribution and the high wall-normal RMS velocity fluctuations observed in the experiment by Kulick et al. (1994) is investigated, and causes for poor agreement between earlier simulations and experiment are explained.

CHAPTER 7

Ideas for future work

1. Overview

The final results for the case of 70 μm particles in a channel flow at $Re_\tau = 644$, presented in the last paper, Paper 7, are in reasonably good agreement with the experimental data by Kulick et al. (1994). For instance, the mean and wall-normal RMS values of the particle velocity are in excellent agreement in most regions of the channel. The location of the peak of RMS value and behavior of bimodal distribution of the streamwise particle velocity are correctly predicted. However, there are two significant discrepancies between data from present numerical simulation and those from experiment: 1) in mean velocity in the vicinity of the wall, say $y^+ < 10$; 2) in RMS streamwise velocity in the logarithmic region.

As discussed in the paper, different behaviors of particles in the vicinity of the wall may result in totally different structures of the flow in the whole channel. Some effects which would work near the wall and are neglected in the present study, may be responsible for these discrepancies. In the following sections, discussion about such considerable effects are made and some results from test computations are presented.

2. Individual topics

2.1. Drag force near the wall. The exact solution by Brenner (1961), Eq. (61), as well as the model formula proposed in the present study, Eq. (63), is based on an assumption that the particle Reynolds number, Re_p, is sufficiently smaller than unity. Therefore, these expressions are not valid for the cases with higher Re_p.

Hallouin et al. (1998) experimentally studied the motion of a glass or steel particle falling in a quiescent fluid down toward a horizontal plane wall. Different sizes and densities of particle were tested. The results were presented as different particle trajectories for different values of the initial particle Reynolds number, Re_{p0}, i.e. Re_p when the particle is moving in a region far from the wall at its terminal velocity. According to those trajectories, increase of the drag near the wall was found to follow the exact solution by Brenner (1961) when Re_{p0} was smaller than about 0.2, and the drag increase was not observed when Re_{p0} was larger than about 4. For the intermediate particle Reynolds numbers, $0.2 < Re_{p0} < 4$, the

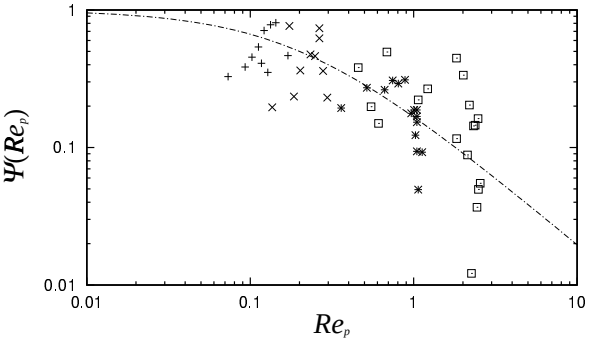

FIGURE 7.1. Values of $\Psi(Re_p)$ extracted from the experimental data by Hallouin et al (1998). +, $Re_{p0} = 0.2$; ×, $Re_{p0} = 0.33$; ∗, $Re_{p0} = 1.1$; □, $Re_{p0} = 2.5$; – - –, curve fit, Eq. (116).

increase of the drag was found to exist but weaker than that can be predicted by Brenner's expression.

Unfortunately, Hallouin et al. (1998) did not present a formula of drag correction factor for the intermediate particle Reynolds number. One can, however, attempt to propose a formula using their data, i.e. by extracting the relation between the drag force, the instantaneous Re_p and the distance from the wall. Here, for example, the form of correction factor near the wall, $C_{w2}(Re_p, \xi)$, is assumed as

$$C_{w2}(Re_p, \xi) = 1 + \Psi(Re_p)(C_{w2} - 1) \ , \tag{114}$$

where C_{w2} is the correction factor for the case of $Re \to 0$, i.e. Eq. (61) or Eq. (63). The unknown function, $\Psi(Re_p)$, takes a value of 0 when $Re_p \to \infty$ and a value 1 when $Re_p \to 0$. This form of function ensures the following asymptotical behaviors,

$$C_{w2}(Re_p, \xi) = \begin{cases} C_{w2} & for \quad Re_p \to 0 \ , \\ \\ 1 & for \quad Re_p \to \infty \ . \end{cases} \tag{115}$$

The values of $\Psi(Re_p)$ extracted from the trajectories for Re_{p0} equal to 0.2, 0.33, 1.1 and 2.5 (Hallouin et al. 1998) are shown in Fig. 7.1. Although large fluctuations can be found in the plots, $\Psi(Re_p)$ can be expressed, from a curve fitting, as

$$\Psi(Re_p) = \frac{1}{1 + 5\ Re_p} \ . \tag{116}$$

The model formula can then be proposed as

$$C_{w2}(Re_p, \xi) = 1 + \frac{C_{w2} - 1}{1 + 5\ Re_p} \ , \tag{117}$$

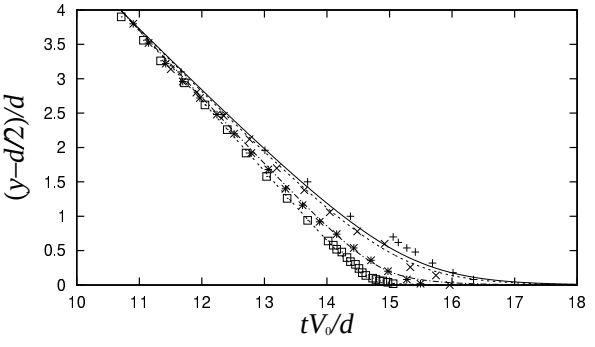

FIGURE 7.2. Trajectory of a particle normalized using terminal velocity, V_0, and particle diameter, d . +, $Re_{p0} = 0.2$; ×, $Re_{p0} = 0.33$; ∗, $Re_{p0} = 1.1$; □, $Re_{p0} = 2.5$; experimental data by Hallouin et al. (1998). Lines, the present simulations using Eq. (117).

Fig. 7.2 shows the trajectory of a particle computed using the proposed model formula, Eq. (117), with the same parameters as those in the experiment by Hallouin et al (1998). The computed trajectories are in reasonably good agreement with the experimental ones.

2.2. Lift forces. In the simulations presented in Paper 7, lift forces are not taken into account. For implementation of the lift forces in the future work, an expression relevant for this case should be known.

Saffman's expression (Saffman, 1965, 1968) was derived with the following restrictions:

- the particle Reynolds number, Re_p, is much smaller than unity, i.e.

$$Re_p << 1 \ , \tag{118}$$

- Re_p is much smaller than the square root of the particle Reynolds number based on shear, Re_G, i.e.

$$\epsilon = \frac{Re_G^{1/2}}{Re_p} >> 1 \ , \tag{119}$$

where Re_G is defined as

$$Re_G = \frac{d^2}{\nu} \left| \frac{du_1^f}{dx_2} \right| \ , \tag{120}$$

and ϵ is a parameter which expresses the relative importance of the shear on particle. The expression of the Saffman lift, Eq. (56), is known to overestimate the lift force as particle Reynolds number increases.

McLaughlin (1991) relaxed the restriction, Eq. (119), and derived,

$$f_2^{(lift)} = \frac{9}{\pi}\rho^f \nu^{1/2} \left(\frac{d}{2}\right)^2 (u_1^f - u_1^p) \left|\frac{du_1^f}{dx_2}\right|^{1/2} \mathrm{sgn}\left(\frac{du_1^f}{dx_2}\right) J^u \ , \tag{121}$$

where J^u is a function of ϵ. McLaughlin (1991) computed J^u in analytical forms for asymptotically small and large values of ϵ, and proposed it as

$$J^u = \begin{cases} -32\pi^2|\epsilon|^5 \ln(1/\epsilon^2) & for \quad |\epsilon| << 1 \ , \\ \\ 2.255 - 0.6463/\epsilon^2 & for \quad |\epsilon| >> 1 \ , \end{cases} \tag{122}$$

while J^u for intermediate ϵ was given by a table.

To relax also the other restriction, Eq. (118), Mei (1992) proposed a correction factor for Saffman lift by correlating Re_p and Re_G obtained from the numerical simulations by Dandy & Dwyer (1990). Mei's correction factor for the Saffman lift, C_M, is written as

$$C_M = \begin{cases} (1 - 0.3314\alpha_G^{1/2})e^{-Re_p/10} + 0.3314\alpha_G^{1/2} & for \quad Re_p \leq 40 \ , \\ \\ 0.0524(\alpha_G Re_p)^{1/2} & for \quad Re_p > 40 \ , \end{cases} \tag{123}$$

where α_G is defined as

$$\alpha_G = \frac{1}{2}\frac{Re_G}{Re_p} \ . \tag{124}$$

The correction factor by Mei, C_M, may also be applied for the the tensorial expression by Li & Ahmadi, Eq. (57). In this case, the shear Reynolds number should be defined as

$$Re_G = \sqrt{2}(s_{lk}s_{kl})^{1/2}\frac{d^2}{\nu} \ . \tag{125}$$

for consistency.

In wall-bounded flows, as is the case in the present study, the lift force induced by the presence of a wall should also be considered. Vasseur & Cox (1977) derived, using an Oseen approximation for the advection term in the Navier-Stokes equation, an expression for the migration velocity, V_m, due to the wall-induced lift. When the particle center is located at a distance y from the wall and sedimenting with a velocity at V_s, the migration velocity can be expressed as,

$$V_m = \frac{3\nu d}{8\pi y^2} I + \mathcal{O}(Re_p) \ , \tag{126}$$

where I is defined as

$$I = \int_0^\infty \int_0^{2\pi} \frac{q+s}{q-s}(\exp(-s) - \exp(-q))s \ ds \ d\phi \ , \tag{127}$$

and

$$q^2 = s^2 + i \ Re_l \cos\phi \ . \tag{128}$$

Here Re_l is a Reynolds number defined by

$$Re_l = \frac{y\, V_s}{\nu} \ . \tag{129}$$

Note, in the limit of $Re_p \to 1$, this expression reach asymptotically the expression by Cox & Hsu (1977),

$$V_m = \frac{3}{64} Re_p \, V_s \ . \tag{130}$$

Cherukat & McLaughlin (1990) experimentally proved that the expression by Vasseur & Cox (1977), Eq. (126) is relevant up to $Re_p = 3$.

The wall-induced lift in the presence of shear and solid wall, as is the case of the present study, is more complicated. Cherukat & McLaughlin (1994) derived an expression for the lift force near a wall in a linear shear flow field, as

$$\begin{aligned} \frac{f_2^{(lift)}}{\rho^f (d/2)^2 V_s^2} \quad = \quad & 1.7716 + 0.2160\eta - 0.7292\eta^2 + 0.4854\eta^3 \\ & -(3.2397\eta^{-1} + 1.1450 + 2.0840\eta - 0.9059\eta^2)\Lambda \\ & +(2.0069 + 1.0575\eta - 2.4007\eta^2 + 1.3174\eta^3)\Lambda^2 \ , \end{aligned} \tag{131}$$

where η is the nondimensional distance from the wall, see Eq. (59), and $\Lambda = dVs/(2G)$ is the nondimensional shear. Use of this expression is recommended (Wang et al., 1997) in the region very close to the wall, say $y^+ < 1$. Outside of the viscous sublayer, $y^+ > 5$, McLaughlin (1993) recommended that J^u in Eq. (121) should be replaced by J, expressed as

$$J = J^u - \frac{1.879}{(y^+)^{5/3}} \ . \tag{132}$$

In the intermediate range, the expression by Vasseur & Cox (1977)

$$J = \frac{\pi^2}{16}\left(\frac{11}{6} y^+ - \frac{1}{\epsilon}\right) \ , \tag{133}$$

or a tabulated values by McLaughlin (1993) may be appropriate. Similarly to McLaughlin's expression for the lift force in an unbounded flow, Eq. (121), the expressions above are valid under the restriction, Eq. (119). Unfortunately, to the best of author's knowledge, it seems that a relevant expression for the wall-induced lift valid for a particle at a higher Reynolds number has not been proposed yet.

3. Results from test computations

3.1. Re_p**-dependent drag correction near the wall.** Similarly to the case presented in Paper 7, a flow of air with 70 μm copper particles in a turbulent channel flow at $Re_\tau = 644$ is considered. At the walls, particles are assumed to lose the wall-normal component of their momentum. Wall surface potential is not taken

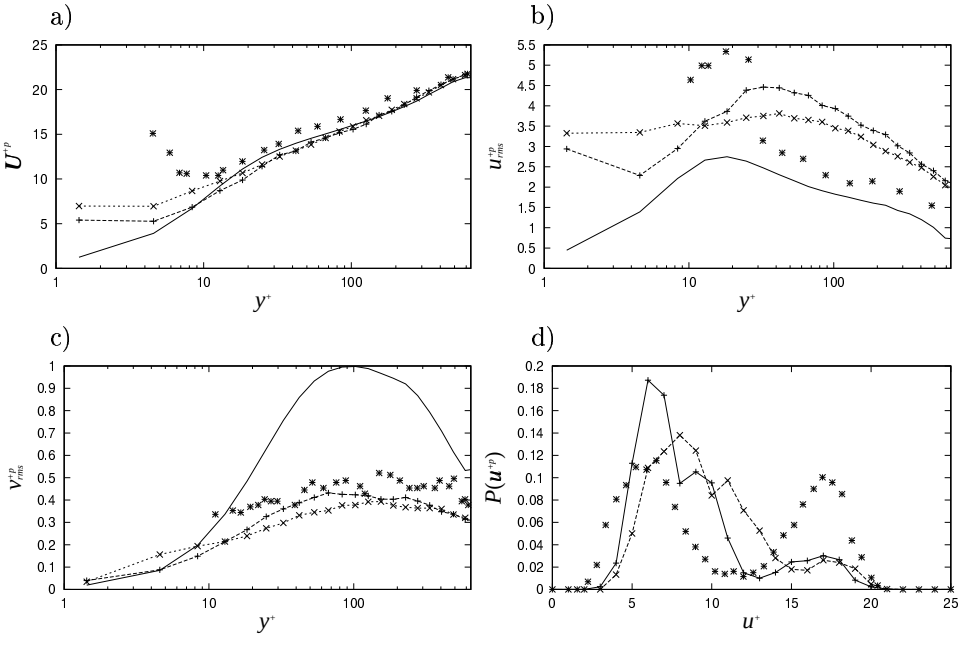

FIGURE 7.3. Particle statistics. a) mean velocity; b) streamwise RMS velocity; c) wall-normal RMS velocity; d) PDF of streamwise velocity. $-+-$, with C_{w2}, Eq. (63) (Case 3 in Paper 7). - - × - -, with $C_{w2}(Re_p, \xi)$, Eq. (117); (1996); $*$, experiment by Kulick et al. (1994), $Z = 2\%$; (———, undisturbed fluid.)

into account. The simulation data obtained using the Reynolds number dependent drag correction near the wall, Eq (117) are compared with those with the original one, Eq (63), i.e. Case 3 in Paper 7.

Here, the mean and RMS values of particle velocities and PDF of particle streamwise velocity are presented in Fig. 7.3a-d. A slight increase in the mean velocity profile, can be observed in the case with the Re_p-dependent drag correction. This is because the high speed particles, whose particle Reynolds number is large, became less influenced by the drag increase near the wall. It can be also observed that the RMS streamwise velocity are flattened in the region $y^+ < 100$. This can be explained, as shown in the PDF of the streamwise velocity, by that the distribution of the lower mode has shifted toward higher values. For the wall-normal RMS velocity only slight change can be observed.

3.2. Lift forces. Test simulations are continued with the same parameters, taking into account the lift force. Saffman lift with Mei's correction is considered.

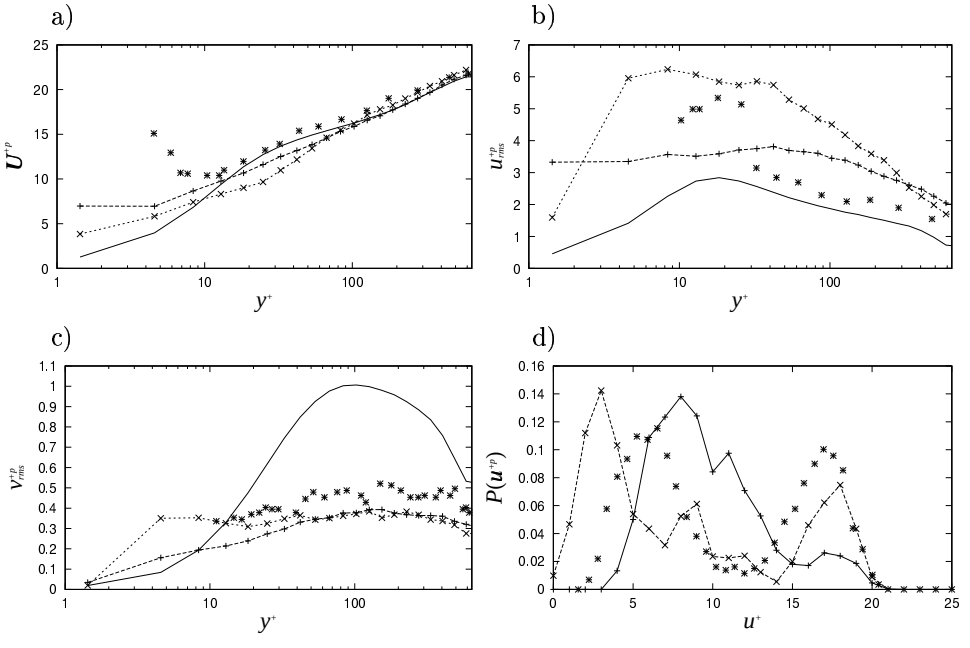

FIGURE 7.4. Particle statistics. a) mean velocity; b) streamwise RMS velocity; c) wall-normal RMS velocity; d) PDF of streamwise velocity. $-+-$, without lift force; - - × - -, with lift force; $*$, experiment by Kulick et al. (1994), $Z = 2\%$; (——–, undisturbed fluid.)

The wall-induced lift is not taken into account because relevant expression for higher particle Reynolds numbers is not found as noted above.

The mean and RMS values of particle velocities and PDF of particle streamwise velocity are presented in Fig. 7.3a-d. Slight decrease of mean velocity profile can be observed when the lift force is considered. From the PDF of streamwise velocity, it can be noticed that the slip-shear lift force has an effect to separate the higher and the lower modes. Due to that, higher streamwise RMS velocity can be observed. The wall-normal RMS velocity was unchanged in most region of the channel, except for increase near the wall.

The present results indicate again that the various force working only near the wall may largely influence whole statistics. Therefore more careful treatment must be done in order to predict such flows with a better accuracy as compared to that presented in Paper 7. However, as mentioned above, there are many problems to overcome, e.g. to find a relevant expression for wall-induced lift for higher particle Reynolds numbers, a challenge which will be left for the future work.

CHAPTER 8

General conclusions

The subject of the present thesis, i.e. particulate turbulent flow, is an ancient subject in the nature. Despite that, due to extreme difficulties appearing in experimental and theoretical studies of such flows, even relatively simple flows are not well understood.

In this thesis, the attention has been paid to theoretical investigation of dilute particulate channel flows at relatively low Reynolds number. It was illustrated that the methodology was successfully applied to the case of study and accurate predictions could be made.

An important conclusion, in addition to those for the specific topics drawn in the papers attached, is the clear illustration of the complexity of the problem. There are a large number of physical phenomena interacting with each other. A complete and accurate prediction of the flow requires detailed models for those phenomena yet not fully available.

Also, one can notice a lack of experience on numerical simulation of such flows in comparison with that of pure turbulent channel flow where a general agreement on simulation parameters is establised between different researching groups. The scientific society has still a long way to go before a complete understanding of turbulent particulate flows with wall interactions can be achieved.

Acknowledgment

I wish to thank my supervisors in Sweden and Japan, Professor Fritz H. Bark, Professor Shunsuke Kondo and Docent Said Zahrai for making this work possible despite all practical complications.

Fritz has always been encouraging me and leading me to a right direction. I had the greatest opportunity to be one of the starting members of FaxénLaboratoriet.

Said, despite his hyper-schedule, spent much time for me not only for the discussions about my research but also for everything during my stay in Sweden.

Kondo-sensei, kindly permitted me to hand in this thesis which also includes parts of my work in Tokyo. I wish to thank him for giving me this opportunity.

The computations for Paper 2, Paper 4 and Paper 5 were done on IBM RS6000 Workstations at ABB Corporate Research, Västerås. Part of the computation for Paper 1 was done on a Sun Workstation at Department of Mechanics, KTH. The other computations, i.e. Paper 3, Paper 6, Paper 7 and part of Paper 1, were done on a DEC AlphaServer 4100 5/466 at Department of Quantum Engineering and Systems Science, University of Tokyo.

For the economical support, FaxénLaboratoriet, which is a cooperative research center supported by KTH, NUTEK and a number of Swedish companies including ABB Corporate Research, and Axel och Margaret Ax:son Johnsons Stiftelse are greatly acknowledged.

I would also like to thank the colleagues at KTH, ABB Corporate Research and University of Tokyo for all fruitful discussions I had.

Finally, I thank my parents and my brother for their encouragement, and my wife, Chiharu, for her love and extensive support.

Bibliography

[1] Amsden, A. A. & Harlow, F. H., 1970. The SMAC method: a numerical technique for calculating incompressible fluid flows. LA-4370, Los Alamos Lab..

[2] Balachander, S. & Maxey, M. R., 1989. Methods for evaluating fluid velocities in spectral simulations of turbulence. *J. Comput. Phys.* **83**, 96-125.

[3] Basset, A. B., 1888. *Treatise on Hydrodynamics* Vol. 2, Chap. 22, pp. 285-297, Deighton Bell, London.

[4] Boehme, G., Krupp, H. & Schnabel, W., 1969. In *Molecular Processes on Solid Surfaces*, Eds. Dranflis et al., McGraw-Hill.

[5] Boguslawski, L. & Popiel, C. O., 1979. Flow structure of the free round turbulent jet in the initial region. *J. Fluid Mech* **99**, 531.

[6] Bolio, E. J. & Sinclair, J. L., 1995. Gas turbulence modulation in the pneumatic conveying massive particles in vertical tubes. *Int. J. Multiphase Flow* **21**, 985-1001.

[7] Bolio, E. J., Yasuna, J. A. & Sinclair, J. L., 1995. Dilute turbulent gas-solid flow in risers with particle-particle interactions. *AIChE J* **41**, 1375-1388.

[8] Boussinesq, J., 1903. *Theorie Analytique de la Chaleur* Vol. 2, p. 224, L'Ecole Polytechnique, Paris.

[9] Brenner, H., 1961. The slow motion of a sphere through a viscous fluid towards a plane surface. *Chemical Engineering Science* **16**, 242-251.

[10] Bretherton, F. P., 1962. The motion of rigid particles in a shear flow at low Reynolds number. *J. Fluid Mech.* **14**, 284-304.

[11] Buevich, Y. A., 1966. *Fluid Dynam.* **1**, 119.

[12] Canuto, V. M. & Cheng, Y., 1997. Determination of the Smagorinsky-Lilly constant C_S. *Phys. Fluids* **9**, 1368-1378.

[13] Cao, J. & Ahmadi, G., 1995. Gas-particle two-phase turbulent flow in a vertical duct. *Int. J. Multiphase Flow* **21**, 1203-1228.

[14] Chandrasekhar, S., 1943. Stochastic problems in physics and astronomy. *Rev. Modern Phys.* **15**, 20-44.

[15] Chen, C. P. & Wood, P. E., 1985. A turbulent closure model for dilute gas-particle flows. *Can. J. Chem. Engng* **63**, 349-360.

[16] Cherukat, P. & McLaughlin, J. B., 1990. Wall-induced lift on a sphere. *Int. J. Multiphase Flow* **16**, 899-907.

[17] Cherukat, P. & McLaughlin, J. B., 1994. The inertial lift on a rigid sphere in a linear shear flow field near a flat wall. *J. Fluid Mech* **263**, 1-18.

[18] Chu, B., 1967. *Molecular Forces:* Based on the Baker Lectures of Peter J. W. Debye, Wiley-Interscience, New York.

[19] Corrsin, S. & Lumley, J., 1956. *Appl. Sci. Res. A* **6**, 114.

[20] Cox, R. G. & Hsu, S. K., 1977. The lateral migration of solid particles in a laminar flow near a plane. *Int. J. Multiphase Flow* **3**, 201-222.

[21] CROWE, C. T., SHARMA, M. P. & STOCK, D. E., 1977. The particle-source-in-cell (PSI-CELL) model for gas-droplet flows. *ASME Trans. J. Fluids Eng.* June.

[22] DANDY, D. S. & DWYER, H. A., 1990. A sphere in shear flow at finite Reynolds number: effect of shear on particle lift, drag, and heat transfer. *J. Fluid Mech.* **216**, 381-410.

[23] DAVIES, C. N., 1945. *Proc. Phys. Soc.* **57**, 259.

[24] DAHNEKE, B., 1972. The influence of flattening on the adhesion of particles. *J. Colloid Interface Sci.* **40**, 1.

[25] Deardorff, J. W., 1970. A numerical study of three-dimensional turbulent channel flow at large Reynolds number. *J. Fluid Mech.* **41**, 453-480.

[26] ELGHOBASHI, S. & TRUESDELL G. C., 1992. Direct simulation of particle dispersion in a decaying isotropic turbulence. *J. Fluid Mech.* **242**, 655-700.

[27] ESMAEELI, A. & TRYGGVASON, G., 1998. Direct numerical simulations of bubbly flows. Part 1. Low Reynolds number arrays. *J. Fluid Mech.* **377**, 313-345.

[28] FAXÉN, H., 1923. Die Bewegung einer starren Kugel Längs der Achse eines mit zaher Flüsigkeit fefüllten Rohres. *Arkiv Mat. Astron. Fys.* **17** (27), 1-28.

[29] FAXÉN, H., 1924. Det Widerstand gegen die Bewegung einer'starren Kugel in einer zähen Flüssigkeit, die zwischen zwei parallelen, ebener Wänden eigeschlossen ist. *Arkiv Mat. Astron. Fys.* **18** (29), 3.

[30] FESSLER J. R., KULICK J. D. & EATON J. K., 1994. Preferential concentration of heavy particles in a turbulent channel flow. *Phys. Fluids* **6**, 3742-3749.

[31] Friedlander, S. K., 1977. *Smoke, Dust and Haze*, p. 45, Wiley & Sons.

[32] GAVIN, L. B., NAUMOV, V. A. & NIKULIN, N. M., 1983. Use of an equation describing the transport of the energy of turbulent pulsations to calculate two-phase jets. *Fluid Dynam.* **16**, 34.

[33] GORE, R. & CROWE, C., 1989. Effect of particle size on modulating turbulent intensity. *Int. J. Multiphase Flow* **15**, 279-285.

[34] GERMANO, M., PIOMELLI, U., MOIN, P. & CABOT, W. H., 1991. A dynamic subgrid-scale eddy viscosity model. *Phys. Fluids A* **3**, 1760-1765.

[35] HALLOUIN, E., GONDRET, P., LANCE, M. AND PETIT L., 1998. On the motion of a sphere toward a plane surface: from lubrication to bouncing regime. *Proc. 3rd Int. Conf. Multiphase Flow* (CD-ROM), Paper 703, 1-9.

[36] HAMAKER, H. C., 1937. The London-van der Waals' attraction between spheroid particles. *Physica* **4**, 1058.

[37] HETSRONI, G., 1989. Particles-turbulence interaction. *Int. J. Multiphase Flow* **15**, 735-746.

[38] HUANG M.-J. & LEONARD A., 1995. Velocity autocorrelation of decaying isotropic homogeneous turbulence. *Phys. Fluids* **7**, 2455-2464.

[39] JONES, W. P. & LAUNDER, B. E., 1972. The prediction of laminarization with a two-equation model of turbulence. *Int. J. Heat Mass Transfer* **15**, 301.

[40] KAFTORI, D., HETSRONI, G. & BANERJEE, S., 1995. Particle behavior in the turbulent boundary layer. I. Motion, deposition, and entrainment. *Phys. Fluids* **7**, 1095-1106.

[41] KIM, J., MOIN, P. & MOSER, R.,1987. Turbulence statistics in fully developed channel flow at low Reynolds number. *J. Fluid Mech.* **177**, 133-166.

[42] KOLMOGOROV, A. N., 1941. The local structure of turbulence in incompressible viscous fluid for very large Reynolds numbers. *Dokl. Akad. Nauk SSSR* **30** 301-305.

[43] KOSHIZUKA, S., TAMAKO, H. & OKA, Y., 1995. A particle method for incompressible viscous flow with fluid fragmentation. *Comput. Fluid Dynamics J.* **4**, 29-46.

[44] KOSHIZUKA, S., NOBE, A. & OKA, Y., 1998. Numerical analysis of breaking waves using the Moving Particle Semi-implicit method. *Int. J. Numer. Meth. Fluids* **26**, 751-769.

[45] KRAICHNAN R. H., 1970. Diffusion by a random velocity field. *Phys. Fluid* **13**, 22-31.

[46] KULICK, J. D., FESSLER, J. R. & EATON, J. K., 1994. Particle response and turbulence modification in fully developed channel flow. *J. Fluid Mech.* **277**, 109-134.

[47] LEE, S., & DURST, F., 1982. On the motion of particles in turbulent duct flows. *Int. J. Multiphase Flow* **8**, 125-146.

[48] LESIEUR, M., 1997. *Turbulence in Fluids* 3rd revised and enlarged edition, Kluwer, Dordrecht.

[49] LI, A. & AHMADI, G., 1993. Deposition of aerosols on surfaces in a turbulent channel flow. *Int. J. Engng Sci.* **31**, 435-451.

[50] LI, A., AHMADI, G., BAYER, R. G. & GAYNES, M. A., 1993. A digital simulation method for estimating dust deposition in a complex geometry passage. *Advances in Electronic Packaging*, ASME, EEP-Vol.4-1, 411-417.

[51] LILLY, K., 1967. The representation of small-scale turbulence in numercal simulation of turbulence, *Proc. IBM Sci. Comput. Symp. Envir. Sci.* IBM Form 320-1951, 195-210.

[52] LILLY, D. K., 1992. A proposed modification of the Germano subgrid scale closure method *Phys. Fluids A* **4** 633-635.

[53] LIU, B. Y. H. & AGARWAL J. K., 1974. Experimental observation of aerosol deposition in turbulent flow. *Aerosol Sci.* **5**, 145-155.

[54] MAEDA, M., HISHIDA, K. & FURUTANI, T., 1980. Optical measurements of local gas and particle velocity in an upward flowing dilute gas-solids suspension. *Polyphase Flow and Transport Technology* Century 2-ETC, pp. 211-216.

[55] MAXEY, M. R. & RILEY, J. J., 1983, Equation of motion for a small rigid sphere in a nonuniform flow. *Phys. Fluids* **26**, 883-889.

[56] MCLAUGHLIN, J. B., 1991, Inertial migration of a small sphere in linear shear flows. *J. Fluid Mech.* **224**, 261-274.

[57] MCLAUGHLIN, J. B., 1993, The lift on a sphere in wall-bounded linear shear flows. *J. Fluid Mech.* **246**, 249-265.

[58] MEI, R., 1992. An approximate expression for the shear lift force on a spherical particle at finite Reynolds number, *Int. J. Multiphase Flow* **18**, 145-147.

[59] MISHIMA, K. & ISHII, M., 1984. Flow regime transition criteria for upward two-phase flow in vertical tubes. *Int. J. Heat Mass Transfer* **27**, 723.

[60] MIYAKE, Y., 1992, In *Suuchi Ryuutai Rikigaku* Eds. Yasuhara & Daiguji, p. 220, Univ. Tokyo Press.

[61] MODERRESS, D., TAN, H. & ELGHOBASHI, S., 1984. Two-component LDA measurement in two-phase turbulent jet. *AIAA J.* **22**, 624-630. Mono-component gases.

[62] NIÑO, Y. & GARCIA, M. H., 1996. Experiments on particle-turbulence interactions in the near-wall region of an open channel flow: implications for sediment transport. *J. Fluid Mech.* **326**. 285-319.

[63] OBOUKHOV, A. M., 1941. On the distribution of energy in the spectrum of turbulent flow. *Dokl. Akad. Sci. Nauk SSSR* **32 A**, 22-24.

[64] O'NEILL, M. E., 1964. A slow motion of viscous liquid caused by a slowly moving solid. *Mathematika* **11**, 67.

[65] OSEEN, C. W., 1927. *Neuere Methoden und Ergebnisse in der Hydrodynamik*, Akademiche Verlag, Leipzig.

[66] OUNIS, H., AHMADI, G. & MCLAUGHLIN, J. B., 1991. Dispersion and deposition of Brownian particles from point sources in a simulated turbulent channel flow. *J. Colloid Interface Sci.* **147**, 233-250.

[67] PAN, Y. & BANERJEE, S., 1996. Numerical simulation of particle interactions with wall turbulence. *Phys. Fluids* **8**, 2733-2755.

[68] PEDINOTTI, S., MARIOTTI, G. & BANERJEE, S., 1992. Direct numerical simulation of particle behaviour in the wall region of turbulent flows in horizontal channels. *Int. J. Multiphase Flow* **15**, 927-941.

[69] PIOMELLI, U., MOIN, P. & FERZIGER, J. H., 1988. Model consistency in large eddy simulation of turbulent channel flow. *Phys. Fluids.* **31**, 1884-1891.

[70] POURAHMADI, F. & HUMPHREY, J. A. C., 1983. Modeling solid turbulent flows. *Physico Chem. Hydrodyn.* 191-219.

[71] POWER, H. & WROBEL, L. C., 1995. *Boundary Integral Methods in Fluid Mechanics*, Computational Mechanics Publications, Southampton, Boston.

[72] PRANDTL, L., 1925. Bericht über Untersuchungen zur ausgebildeten Turbulenz. *ZAMM* **5**, 136-139.

[73] RASHIDI, M., HETSRONI, G. & BANERJEE, S., 1990. Particle-turbulence interaction in a boundary layer. *Int. J. Multiphase Flow* **16**, 935-949.

[74] RILEY, J. J., 1971. Ph.D Thesis, The Johns Hopkins University, Baltimore, Maryland.

[75] RIZK, M. A. & ELGHOBASHI, S. E., 1989. A two-equation turbulence model for dispersed dilute confined two-phase flows. *Int. J. Multiphase Flow* **15**, 119-133.

[76] REEKS, M. W., 1991. On a kinetic equation for the transport of particles in turbulent flows. *Phys. Fluids A* **3**, 446-456.

[77] ROUSON, D. W. I. & EATON, J. K., 1994. Direct numerical simulation of particles interacting with a turbulent channel flow. *Proc. 7th Workshop on Two-phase Flow Predictions,* Erlangen, Germany.

[78] RUBINOW, S. I. & KELLER, J. B., 1961. The transverse force on spinning sphere moving in a viscous fluid. *J. Fluid Mech.* **11**, 447.

[79] SAFFMAN, P. G., 1965. The lift on a small sphere in a slow shear flow. *J. Fluid Mech.* **22**, 385-400.

[80] SAFFMAN, P. G., 1968. Corrigendum to 'The lift on a small sphere in a slow shear flow'. *J. Fluid Mech.* **31**, 624.

[81] SCHILLER, L. & NAUMANN, A., 1933. Über die grundlegenden Berechungen bei der Schwerkraftaufbereitung. *Ver. Deut. Ing.* **77**, 318.

[82] SHIH, T.-H. & LUMLEY, J. L., 1986. Second-order modelling of particle dispersion in a turbulent flow. *J. Fluid Mech.* **163** 349-363.

[83] SIMONIN, O., DEUTSCH, E. & BOIVIN, M., 1995. Large eddy simulation and second-moment closure model of particle fluctuating motion in two-phase turbulent shear flows. *Proc. 9th Int. Symp. Turbulent Shear Flows*, 85-115.

[84] SIMONIN, O., 1996. Continuum modelling of dispersed turbulent two-phase flows. von Karman Institute for Fluid Dynamics, Lecture Series 1996-02.

[85] SMAGORINSKY, J., 1963. General circulation experiments with the primitive equations. *Monthly Weather Rev.* **93**, 99-164.

[86] SOLTANI, M. & AHMADI, G., 1995. Direct numerical simulation of particle entrainment in turbulent channel flow. *Phys. Fluids.* **7**, 647-657.

[87] SOMMERFELD, M., 1999. Inter-particle collisions in turbuloent flows: a stochastic Lagrangian model. *Turbulence and Shear Flow Phenomena - 1*, Eds. Banerjee, S. & Eaton, J. K., 265-270, Begell House Inc., New York, ISBN 1-56700-135-1.

[88] STOCK, D. E., 1996. Particle Dispersion in Flowing Gases — 1994 Freeman Scholar Lecture. *J. Fluids Engng* **118**, 4-17.

[89] SUNDARAM, S. & COLLINS, L. R., 1997. Collision statistics in an isotropic particle-laden turbulent suspension. Part 1. Direct numerical simulations. *J. Fluid Mech.* **335**, 75-109.

[90] SWAILES, D. C. & REEKS, M. W., 1994. Particle deposition from a turbulent flow. I. A steady-state model for high inertia particles. *Phys. Fluids* **6**, 3392-3403.

[91] TANAKA, T. & TSUJI, Y., 1991. Numerical simulation of gas-solid two-phase flow in a vertical pipe: on the effect of inter-particle collision. *ASME/FED Gas-Solid Flows*, 123-128.

[92] TENNEKES, H. & LUMLEY, J. L., 1975. *A first course in turbulence*, MIT Press, Cambrige.

[93] TCHEN, C.-M., 1947. Mean value and correlation problems connected with the motion of small particles suspended in a turbulent fluid. Ph.D thesis, De technische hogeschool te Delft.

[94] TSUJI, Y., MORIKAWA, Y. & SHIOMI, H., 1984. LDV measurement of an air-solid two-phase flow in a vertical pipe. *J. Fluid Mech.* **139** 417-434.

[95] WIJTTEWAAL, W. S. J. & OLIEMANS, R. V. A., 1996. Particle dispersion and deposition in direct numerical and large eddy simulations of vertical pipe flows. *Phys. Fluids* **8** 2590-2604.

[96] VASSEUR, P. & COX, R. G., 1977. The lateral migration of spherical particles sedimenting in a stagnant bounded fluid. *J. Fluid Mech.* **80**, 561-591.

[97] WAKIYA, S. J., 1960. Research Report 9, Faculty of Engineering, Niigata Univ., Japan.

[98] WALL, T. F., SUBRAMANIAN, V. & HOWLEY, P., 1982. An experimental study of the geometry mixing and entrainment of particle laden jets up to ten diameters from the nozzle. *Trans. Inst. Chem. Eng.* **60**, 231.

[99] WANG, Q. & SQUIRES, K. D., 1996a. Large eddy simulation of particle deposition in a vertical turbulent channel flow. *Int. J. Multiphase Flow* **22**, 667-683.

[100] WANG, Q. & SQUIRES, K. D., 1996b. Large eddy simulation of particle-laden turbulent channel flow. *Phys. Fluids.* **8**, 1207-1223.

[101] WELLS, M. R. & STOCK, D. E, 1983. The effects of crossing trajectories on the dispersion of particles in a turbulent fluid. *J. Fluid Mech.* **136**, 31-62.

[102] WOOD, N. B., 1981. The mass transfer of particles and acid vapour to cooled surfaces. *J. Inst. Energy* **76**, 76-93.

[103] YAMAMOTO, Y., TANAKA, T. & TSUJI, Y., 1998. LES of gas-particle turbulent channel flow (The effect of inter-particle collision on structure of particle distribution). *Proc. 3rd Int. Conf. Multiphase Flow* (CD-ROM), Paper 518, 1-7.

[104] YEUNG, P. K. & POPE, S. B., 1988. An algorithm for tracking fluid particles in numerical simulations of homogeneous turbulence. *J. Comput. Phys.* **79**, 373-416.

[105] YONEMURA, S., TANAKA, T. AND TSUJI, Y., 1993. Cluster formation in gas-solid flow predicted by the DSMC method. *ASME/FED Gas-Solid Flows*, 303-309.

[106] YUAN, Z. & MICHAELIDES, E. E., 1992. Turbulence modulation in particulate flows - a theoretical approach. *Int. J. Multiphase Flow* **18**, 779-785.

[107] ZAHRAI, S., BARK, F. H. & KARLSSON, R. I., 1995. On anisotropic subgrid modeling. *Eur. J. Mech., B/Fluids* **14**, 459-486.

[108] ZISSELMAR, R. & MOLERUS, O., 1979. Investigation of solid-liquid pipe flow with regard to turbulence modification. *Chem. Eng. J.* **18**, 233-239.